Computational Mechanics manuscript No.
(will be inserted by the editor)

Efficient formulations of the material identification problem using full-field measurements

Jorge M. Pérez Zerpa · **Alfredo Canelas**

Received: date / Accepted: date

Abstract The material identification problem addressed consists of determining the constitutive parameters distribution of a linear elastic solid using displacement measurements. This problem has been considered in important applications such as the design of methodologies for breast cancer diagnosis. Since the resolution of real life problems involves high computational costs, there is great interest in the development of efficient methods. In this paper two new efficient formulations of the problem are presented. The first formulation leads to a second-order cone optimization problem, and the second one leads to a quadratic optimization problem, both allowing the resolution of the problem with high efficiency and precision. Numerical examples are solved using synthetic input data with error. A regularization technique is applied using the Morozov criterion along with an automatic selection strategy of the regularization parameter. The proposed formulations present great advantages in terms of efficiency, when compared to other formulations that require the application of general nonlinear optimization algorithms.

Keywords Identification · Inverse problems · Kinematic field measurements · Second-order cone programming

1 Introduction

The direct linear elasticity problem of solid mechanics consists of obtaining the displacement, strain and stress fields inside an elastic body. External loads, supports and the material properties of the elastic body are considered known. However, in certain important applications the material properties are unknown, and must be estimated from measurements of

J. M. Pérez Zerpa (✉) · A. Canelas
Instituto de Estructuras y Transporte
Facultad de Ingeniería, Universidad de la República
Accepted version accepted and published at https://doi.org/10.1007/s00466-016-1291-1

displacements, strains and stresses caused by a known external action, i.e. a Material Identification Problem (MIP) must be formulated and solved. The reader may find an extensive survey about the theoretical aspects and practical solution strategies for the MIP and other inverse problems in Elasticity in [9].

One of the applications where MIPs are formulated is in structural damage identification [29,38,41]. The MIPs are also formulated in the development of new techniques for diagnosis of diseases, in situations where the tissue health can be inferred from its constitutive material properties [23,15,42]. Motivated by these important applications, several groups of researchers in the scientific community have made a great effort in the development of new methods for the solution of the MIP. This article contributes with two new formulations for the MIP, along with their respective efficient solution methodologies.

The MIP, like other inverse problems, is an *ill-posed* problem, i.e. the solution does not satisfy all the Hadamard conditions: existence, uniqueness and continuous dependence on the given data [27]. There have been some recent results about the existence and uniqueness of the solution in certain MIPs, such as sufficient conditions for an incompressible solid [6], and for a compressible solid under dynamical tests using complete displacement information [33]. However, one of the main challenges of the MIPs, as well as other *ill-posed* inverse problems in engineering, is the high sensitivity of the solution with respect to measurement errors in the given data, which are invariably present. On the other hand, large scale real life problems are still challenging for the most frequently used MIP methods, and the high computational costs associated to practical applications have fueled intense research on new efficient methods of solution. Since the contribution made by Ophir et al. where Elastography is presented [35] to the recent results in [23], there has been an important advance in the development of new techniques for one of the most important applications: breast cancer diagnosis.

A brief bibliographical review of the historical development of MIP resolution methods is presented in the following. The papers [26,12] are among the first references dealing with mechanical parameters identification problems where optimization problems are formulated and solved. In [35] the Elastography is presented as a technique that allows the estimation of material properties, using data obtained by applying ultrasound technology. In [25,16] the identification of mechanical properties of tissues is performed by formulating and solving an optimization problem. In this kind of formulation the design variables are values of the mechanical properties of each part of certain partition of the solid and the objective functional is a measure of the distance between the experimentally measured displacements and the displacements provided by a numerical model, i.e. if the vector $\mathbf{x}$ represents the set of n unknown mechanical parameters, the optimization problem is:

$$\min_{\mathbf{x}\in\mathbb{R}^n} \|\mathbf{U}(\mathbf{x}) - \mathbf{U}^m\|^2. \tag{1}$$

where $\mathbf{U}^m$ is the vector of measured displacements and $\mathbf{U}(\mathbf{x})$ is the vector of the same displacements computed by certain numerical method. An iterative optimization algorithm is used to find an optimal solution. A survey of iterative methods for general material identification is presented in [15]. Gradient-based techniques [32] are usually applied, as in [14, 11] where the authors identify the Young modulus in arteries. In other material identification articles derivative-free algorithms are used [38]. A previous analysis must be done to determine which type of algorithm should be used for each application, taking into account the differences between the diverse optimization strategies available [1].

A particular case of MIP arises when complete information of the displacement field of the body is at hand. The Full-field Measurement (FFM) methods were developed in the last decades for this case. In these methods the displacements of all the nodes in a given mesh are assumed known. Since the development of new image processing techniques and the availability of equipments at accessible prices, the use of FFM-based methods has increased. Avril et. al [3] present an extensive overview of FFM methods. These methods have been applied to the characterization of several materials, such as alloy plates [3], PVC plates [37], and even Biomechanics applications [2, 23]. In this article we will focus on the development of numerical methods based on FFM data.

Our goal is to propose new formulations capable to obtain an important reduction of the time required by the MIP resolution without losing precision in the solution. In order to achieve this goal, the formulations should admit the use of known efficient optimization algorithms, and the application of effective regularization techniques.

Unidimensional example

In order to look for efficient formulations we start with a simple question: What norms are the most appropriate for the problem formulated in Equation (1)? A simple unidimensional example is considered here to illustrate the importance of using a convenient formulation of the MIP.

Let us consider a bar with length ℓ and constant cross-sectional area A. The left section of the bar is fixed and a load $P = 1$ N is applied on the right section. The direct elasticity problem is solved numerically using a discretization of $n_E = 20$ finite elements with equal size and with a known Young modulus E_i at each element i. In this case, given the nodal displacements, the MIP consists of obtaining the Young modulus at each element. The reference displacements $\mathbf{U}^r$ are computed as the solution of the direct problem using the Young modulus distribution E^r, which is given by: $E = 1$ Pa for the first 10 elements and $E = 2$ Pa for the following 10 elements (from left to right).

The inverse problem is formulated as the following optimization problem:

$$\min_{\mathbf{E}\in\mathbb{R}^{n_E}} \quad \|\mathbf{U}(\mathbf{E}) - \mathbf{U}^m\|^2 + \alpha\mathscr{R}(\mathbf{E}) \tag{2}$$

where $\mathbf{U}^m$ are the measured displacements (which can differ from $\mathbf{U}^r$ due to the presence of errors), $\mathscr{R}(\mathbf{E})$ is a regularization term and α is the regularization parameter that determines the weight of the regularization term in the cost functional. We also consider that each Young modulus E_i belongs to the known interval $I_E = [0.5, 2.5]$.

Let us start with a reformulation of Problem (2) in the following equivalent way:

$$(\text{FU}) \begin{cases} \min\limits_{\mathbf{E},\mathbf{U}} & \|\mathbf{U}-\mathbf{U}^m\|^2 + \alpha\mathscr{R}(\mathbf{E}) \\ \text{s.t.} & \\ & \mathbf{K}(\mathbf{E})\mathbf{U} = \mathbf{F} \\ & \mathbf{E} \in \mathbf{I}_E^{n_E} \quad \mathbf{U} \in \mathbb{R}^{n_U} \end{cases} \tag{3}$$

where $\mathbf{K}$ and $\mathbf{F}$ are the stiffness matrix and external load vector, respectively, obtained through the application of the finite element discretization, and n_U is the number of degrees of freedom (in this example $n_E = n_U = 20$). An alternative formulation is given by the following expression:

$$(\text{FR}) \begin{cases} \min\limits_{\mathbf{E},\mathbf{R}} & \|\mathbf{R}\|^2 + \alpha\mathscr{R}(\mathbf{E}) \\ \text{s.t.} & \\ & \mathbf{K}(\mathbf{E})\mathbf{U}^m = \mathbf{F} + \mathbf{R} \\ & \mathbf{E} \in \mathbf{I}_E^{n_E} \quad \mathbf{R} \in \mathbb{R}^{n_U} \end{cases} \tag{4}$$

where $\mathbf{R}$ is a residual load vector introduced to eliminate the $\mathbf{U}$ variable. In both formulations $\|\cdot\|$ represents a norm in $\mathbb{R}^{n_U}$. In this example we will see the advantages and disadvantages of each formulation when the euclidean norm is considered, comments will be made about the use of other norms in the following section.

The formulation FU is equivalent to the one given by Equation (2), and using the euclidean norm it is one of the most used formulations of the literature. Note that the equality constraints of FU are nonlinear and define a nonconvex feasible set. Hence, in spite of the simplicity of the formulation, general algorithms for nonlinear optimization problems must be used to solve it, and the solution found could be a local minimum, i.e. a bad-quality solution far away from the global minimum.

The formulation FR has a convex quadratic cost functional (for euclidean norm) and its constraints are linear, thus the optimization problem is a convex quadratic programming problem. For these problems there exist very efficient algorithms for obtaining a global minimum [8].

Let us compare the solutions of FU and FR when data with error ($\mathbf{U}^m$) is used. The displacements $\mathbf{U}^m$ are computed as the solution of the direct problem using a Young modulus distribution E^m, different from E^r. E^m is given by: $E = 1$ Pa for the first 10 elements, $E = 3$ Pa for the 11-th element and $E = 2$ Pa for the following 9 elements. This distribution has a 50% error in the 11-th element, therefore errors are introduced in $\mathbf{U}$. For both formulations the euclidean norm was used. When the optimization problem is solved without considering

the regularization term ($\alpha = 0$), we obtain the results presented in Figure 1(a). The figure

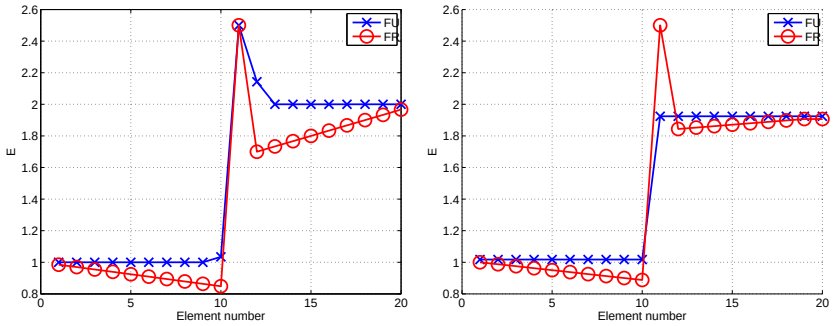

(a) results obtained without regularization (b) results obtained with regularization

Fig. 1 Results unidimensional example.

shows that the constraint $E_{11} \leq 2.5$ Pa becomes active at the solution, and that the values obtained for E in the elements around the 11-th element present a considerable error. The effect of the active constraint is much more negative for the formulation FR.

Let us consider now a regularization term given by the Total Variation cost functional (TV) that will be discussed later (see Equation (39)). To choose an appropriate regularization parameter α, the Morozov criterion is applied in a similar fashion as in [23]. The values obtained are $\alpha = 0.018$ for the FU formulation and $\alpha = 0.044$ for the FR formulation, and in both cases the respective Morozov parameter is $M(\alpha) = 0.99$. The Morozov parameter will be introduced in Section 2.4.

The results obtained are presented in Figure 1(b), where we can see the effect of the regularization term in the solution. The solution of FU is highly improved, providing for a correct identification of the reference E. However, the regularization does not produce a similar effect in the solution of FR. The solution for the best value of α has almost the same error in E_{11}. A larger value of α can decrease the value of E_{11}, but decreases also the values of E in the elements 12 to 20, producing an increase of the global error of the solution.

In short, there are three main aspects that can be used to compare formulations FU and FR: convexity, computational cost, and applicability of regularization. The formulation FR is convex, so that it cannot present non-global local minima, which represents an important advantage over FU. Another important advantage of FR is that it admits the use of specific very efficient optimization algorithms, whereas FU requires the use of algorithms for general nonlinear optimization problems. The last aspect presents a critical disadvantage of FR. The results obtained show that the TV regularization cannot be successfully applied to the FR formulation, so that the FR, in its actual form, cannot be reliably used to solve the MIP.

In the comparison presented above the euclidean norm was considered in the objective functional of both formulations. This means the objective functionals were defined after discretization, so that their values can strongly depend on the particular mesh used, as well as the solution of the optimization problem. To avoid a strong mesh dependence, the identification formulation should be stated instead in the continuous setting. In the search for new appropriate formulations of the MIP we will try to get the following features:

- convexity: the optimization problem should be ideally convex,
- continuum formulation: the formulation should be established before the domain discretization to avoid a strong mesh dependence of the solution,
- efficiency: the solution should be obtained efficiently. Then, known efficient algorithm of solution for large scale problems should be available,
- regularization: the formulation should admit a regularization technique to reduce the effect of the error in the data over the solution.

In the following section new formulations satisfying the above requirements are presented. In Section 3 numerical results are presented showing the efficiency of the proposed formulations and conclusions are presented in Section 4.

2 Formulations of the material identification problem

In this section we describe several known formulations of the MIP and also introduce new formulations taking into consideration the desired features listed above. The formulations are stated for the two-dimensional case, but admit straightforward generalizations for three-dimensional problems. We start by describing the Linear Elasticity Problem (LEP), which will be our direct problem. Then the MIP formulations are presented as optimization problems in a continuous domain with their respective discrete versions.

2.1 Linear Elasticity Problem: direct problem

Let us consider a linear elastic solid occupying the region Ω with boundary $\partial\Omega$. The boundary is a disjoint union of $\Gamma_{\mathbf{t}}$ and $\Gamma_{\mathbf{u}}$, i.e. $\partial\Omega = \Gamma_{\mathbf{u}} \cup \Gamma_{\mathbf{t}}$ and $\Gamma_{\mathbf{u}} \cap \Gamma_{\mathbf{t}} = \emptyset$. In $\Gamma_{\mathbf{t}}$ the surface loads are given by the known vector field $\hat{\mathbf{t}}$, whilst in $\Gamma_{\mathbf{u}}$ the displacements are given by $\hat{\mathbf{u}}$. A plane strain state is assumed, with zero external volume loads.

2.1.1 Strong formulation

In the strong formulation of the LEP, the symmetric Cauchy stress tensor $\boldsymbol{\sigma}$ must satisfy the equilibrium equations given by Equation (5a) and the boundary conditions given by Equation (5d). The solid is formed by a linear elastic heterogeneous material, therefore the

strain-stress relation is given by the known fourth-order tensor field $\mathbb{C}$ and the constitutive equation (5b), where $\boldsymbol{\varepsilon}$ is the infinitesimal strain tensor. The tensor $\boldsymbol{\varepsilon}$ must also satisfy the strain-displacement relation given by Equation (5c) and $\mathbf{u}$ must satisfy the boundary conditions given by Equation (5e). These equations define the LEP in its strong form, which consists of finding the displacements field $\mathbf{u} : \Omega \to V^2$, the stress field $\boldsymbol{\sigma} : \Omega \to \text{Sym}$ and the strain field $\boldsymbol{\varepsilon} : \Omega \to \text{Sym}$, that satisfy:

$$\begin{cases} \nabla \cdot \boldsymbol{\sigma} = 0 \text{ in } \Omega & \text{(5a)} \\ \boldsymbol{\sigma} = \mathbb{C}[\boldsymbol{\varepsilon}] \text{ in } \Omega & \text{(5b)} \\ \boldsymbol{\varepsilon} = \dfrac{\nabla \mathbf{u} + \nabla^{\mathrm{T}} \mathbf{u}}{2} \text{ in } \Omega & \text{(5c)} \\ \boldsymbol{\sigma}[\mathbf{n}] = \hat{\mathbf{t}} \text{ on } \Gamma_{\mathbf{t}} & \text{(5d)} \\ \mathbf{u} = \hat{\mathbf{u}} \text{ on } \Gamma_{\mathbf{u}}, & \text{(5e)} \end{cases}$$

where V^2 is the space of two-dimensional vectors and Sym is the space of second-order symmetric tensors.

2.1.2 Weak formulation

The LEP can also be formulated in its weak form. Considering all the hypothesis of the last section for the solid Ω, the weak formulation consists of finding $\mathbf{u} \in \mathscr{U}$ satisfying:

$$a_{\mathbb{C}}(\mathbf{u}, \mathbf{v}) = \ell(\mathbf{v}) \qquad \forall \mathbf{v} \in \mathscr{V} \tag{6}$$

where the bilinear operator $a_{\mathbb{C}}(\mathbf{u}, \mathbf{v})$, given by:

$$a_{\mathbb{C}}(\mathbf{u}, \mathbf{v}) = \int_{\Omega} \mathbb{C}[\boldsymbol{\varepsilon}(\mathbf{u})] : \boldsymbol{\varepsilon}(\mathbf{v}) \, \mathrm{d}V \qquad (\mathbf{u}, \mathbf{v}) \in \mathscr{U} \times \mathscr{V}, \tag{7}$$

represents the internal virtual work, whilst $\ell(\mathbf{v})$ is the external virtual work:

$$\ell(\mathbf{v}) = \int_{\Gamma_{\mathbf{t}}} \mathbf{v} \cdot \hat{\mathbf{t}} \, \mathrm{d}\Gamma \qquad \mathbf{v} \in \mathscr{V}. \tag{8}$$

$\mathscr{U}$ is the set of the kinematically admissible displacements:

$$\mathscr{U} = \left\{ \mathbf{u} \in H_1(\Omega)^2 : \mathbf{u} = \hat{\mathbf{u}} \text{ on } \Gamma_{\mathbf{u}} \right\}, \tag{9}$$

and $\mathscr{V}$ is the set of the virtual displacements:

$$\mathscr{V} = \left\{ \mathbf{v} \in H_1(\Omega)^2 : \mathbf{v} = \mathbf{0} \text{ on } \Gamma_{\mathbf{u}} \right\}. \tag{10}$$

2.2 Material Identification Problem: continuum formulations

Let us consider now that instead of knowing the field of material properties $\mathbb{C}$, we know the displacement field of the solid. This displacement field is measured at each point of the solid and denoted as $\mathbf{u}^m$. Then the general MIP consists of determining the field $\mathbb{C} \in \mathbf{C}$ which characterizes the material that forms the solid, where $\mathbf{C}$ is the set of constitutive tensor fields, defined as in [21]:

$$\begin{aligned}\mathbf{C} = \big\{ &\mathbb{C} \in (L_\infty(\Omega))^{3\times 3}; \mathbb{C} = \mathbb{C}^{\mathrm{T}}, \mathbb{C}[\boldsymbol{\varepsilon}] : \boldsymbol{\varepsilon} \geq \gamma |\boldsymbol{\varepsilon}|^2 \\ &\gamma > 0 \; \forall \boldsymbol{\varepsilon},\ \mathbb{C}[\boldsymbol{\varepsilon}] : \boldsymbol{\varepsilon}' \leq \xi |\boldsymbol{\varepsilon}||\boldsymbol{\varepsilon}'|\ \ \xi > 0\ \ \forall (\boldsymbol{\varepsilon}, \boldsymbol{\varepsilon}') \big\}, \end{aligned} \tag{11}$$

where $L_\infty(\Omega)$ is the space of real measurable bounded functions in Ω.

The characterization problem in the continuum can be written as an optimization problem in the following manner

$$\min_{\mathbb{C}\in\mathbf{C}} \quad \mathscr{J}(\mathbf{u}(\mathbb{C}) - \mathbf{u}^m) \tag{12}$$

where $\mathbf{u}(\mathbb{C})$ is the solution of the direct problem of Equation (6) for the field $\mathbb{C}$.

As it was seen in the unidimensional example, the quality of the MIP solution obtained depends on the formulation used. In the following section we will describe two of the most used formulations at the moment as well as introduce new proposals. We will show that the new proposed formulations have the recommended features listed in the introduction, producing results with high computational efficiency.

2.2.1 Quadratic Error in displacements

One of the most used formulations is the one we call quadratic error in displacements. This is a widely used formulation defined in the continuum [22, 23, 5] or in the discretized domain as in the formulation FU [16, 11, 18]. Let us consider the error defined in the continuous domain as:

$$\mathscr{J}_2(\mathbb{C}) = \frac{1}{2} \|\mathbf{u}(\mathbb{C}) - \mathbf{u}^m\|^2_{L_2(\Omega)^2} \tag{13}$$

where $\|\cdot\|_{L_2(\Omega)^2}$ is the norm given by

$$\|\mathbf{u}\|_{L_2(\Omega)^2} = \sqrt{\int_\Omega |\mathbf{u}|^2 \, \mathrm{d}V}. \tag{14}$$

2.2.2 Error in Constitutive Equation

In [28] Ladeveze and Leguillon presented a procedure for efficient refinement of FEM meshes using a functional based on a quadratic error in the constitutive law. After that, similar functionals where proposed and used to obtain new MIP formulations, producing

a new class of functionals called Error in Constitutive Equation (ECE). One of the most remarkable functionals is the one called Constitutive Equation Gap (CEG), given by:

$$\tilde{\mathscr{E}}(\mathbf{w},\boldsymbol{\sigma},\mathbb{C}) = \frac{1}{2}\int_{\Omega} (\boldsymbol{\sigma} - \mathbb{C}[\boldsymbol{\varepsilon}(\mathbf{w})]) : \mathbb{C}^{-1}\left[\boldsymbol{\sigma} - \mathbb{C}[\boldsymbol{\varepsilon}(\mathbf{w})]\right] \mathrm{d}V. \tag{15}$$

being $\mathbf{w} \in \mathscr{U}$ a kinematically admissible displacement field, $\boldsymbol{\sigma} \in \Sigma$ a statically admissible stress field and $\mathbb{C} \in \mathbf{C}$ the constitutive tensor field.

In order to use this functional to solve the MIP, the measured displacement information $\mathbf{u}^m$ must be taken into account. One of the ways to do that is to impose $\mathbf{w} = \mathbf{u}^m$. This variant is called Constitutive Equation Gap Method (CEGM) [17,36], and consists basically of solving the following optimization problem:

$$\min_{\mathbb{C}\in\mathbf{C}} \mathscr{J}_{CEG}(\mathbb{C}) \qquad \mathscr{J}_{CEG}(\mathbb{C}) = \min_{\boldsymbol{\sigma}\in\Sigma} \mathscr{E}(\boldsymbol{\sigma},\mathbb{C}), \tag{16}$$

where the functional $\mathscr{E}$ is obtained by substitution in the definition of $\tilde{\mathscr{E}}$:

$$\mathscr{E}(\boldsymbol{\sigma},\mathbb{C}) = \frac{1}{2}\int_{\Omega} (\boldsymbol{\sigma} - \mathbb{C}[\boldsymbol{\varepsilon}(\mathbf{u}^m)]) : \mathbb{C}^{-1}\left[\boldsymbol{\sigma} - \mathbb{C}[\boldsymbol{\varepsilon}(\mathbf{u}^m)]\right] \mathrm{d}V \tag{17}$$

and Σ is the set of statically admissible Cauchy stress tensor fields. In our case this is equivalent to:

$$\Sigma = \left\{ \boldsymbol{\sigma} \in H^{\mathrm{div}}(\Omega) \,:\, \nabla\cdot\boldsymbol{\sigma} = 0 \text{ in } \Omega,\ \boldsymbol{\sigma}[\mathbf{n}] = \hat{\mathbf{t}} \text{ on } \Gamma_{\mathbf{t}} \right\}, \tag{18}$$

where $H^{\mathrm{div}}(\Omega)$ is:

$$H^{\mathrm{div}}(\Omega) = \{\boldsymbol{\sigma} \in (L^2(\Omega))^4 : \boldsymbol{\sigma} = \boldsymbol{\sigma}^{\mathrm{T}},\ \nabla\cdot\boldsymbol{\sigma} \in (L^2(\Omega))^2\}. \tag{19}$$

In accordance with the results described in [3] it can be said that this is one of the most appropriate functionals for the MIP resolution by the moment. In the last years other variants of methods inspired in the CEGM have been presented, as in [43], however there are still aspects to improve. The functional $\mathscr{E}$ presents important properties for the MIP resolution such as convexity [21], however, we have not seen in the literature formulations of the problem where efficient convex optimization algorithms [8] were applied. That is why in this article we present formulations for addressing this issue.

The resolution of Problem (16) is equivalent to solve the following problem:

$$\min_{(\boldsymbol{\sigma},\mathbb{C})\in\Sigma\times\mathbf{C}} \mathscr{E}(\boldsymbol{\sigma},\mathbb{C}). \tag{20}$$

One of the challenges of these kind of methods is the construction of the set Σ, particularly when high-order finite elements are used. Using the virtual work principle we can rewrite

the problem as:

$$\begin{cases} \min\limits_{\boldsymbol{\sigma},\mathbb{C}} & \mathscr{E}(\boldsymbol{\sigma},\mathbb{C}) \\ \text{s.t.} & \\ & \displaystyle\int_{\Omega} \boldsymbol{\sigma} : \boldsymbol{\varepsilon}(\mathbf{v})\,\mathrm{d}V = l(\mathbf{v}) \quad \forall \mathbf{v} \in \mathscr{V} \\ & \mathbb{C} \in \mathbf{C} \quad \boldsymbol{\sigma} \in H^{div}(\Omega) \end{cases} \tag{21}$$

This form of the problem allow us to introduce a modification which will be presented in the following section.

2.2.3 Quadratic Error in Constitutive Equation

Now let us present a new formulation that can be solved using efficient algorithms as it was done using the formulation FR, maintaining some of the good features of the CEGM. This formulation was not seen by the authors during the research of the literature.

Let us consider the problem where the functional is given by Equation (17) and let us consider $\mathbb{C}^{-1}$ as a known tensor field $(\mathbb{C}^{(k)})^{-1}$. We obtain the modified functional:

$$\mathscr{E}_q^{(k)}(\boldsymbol{\sigma},\mathbb{C}) = \frac{1}{2}\int_{\Omega} (\boldsymbol{\sigma} - \mathbb{C}[\boldsymbol{\varepsilon}(\mathbf{u}^m)]) : \left(\mathbb{C}^{(k)}\right)^{-1} [\boldsymbol{\sigma} - \mathbb{C}[\boldsymbol{\varepsilon}(\mathbf{u}^m)]]\,\mathrm{d}V. \tag{22}$$

Now let us apply the change of variables $\mathbf{s} = \boldsymbol{\sigma} - \mathbb{C}[\boldsymbol{\varepsilon}(\mathbf{u}^m)] \in \mathscr{S}$. Rewriting the problem of Equation (21) we obtain:

$$\begin{cases} \min\limits_{\mathbb{C},\mathbf{s}} & \displaystyle\frac{1}{2}\int_{\Omega} \mathbf{s} : \left(\mathbb{C}^{(k)}\right)^{-1} [\mathbf{s}]\,\mathrm{d}V \\ \text{s.t.} & \\ & \displaystyle\int_{\Omega} \mathbb{C}\,[\boldsymbol{\varepsilon}(\mathbf{u}^m)] : \boldsymbol{\varepsilon}(\mathbf{v})\,\mathrm{d}V + \int_{\Omega} \mathbf{s} : \boldsymbol{\varepsilon}(\mathbf{v})\,\mathrm{d}V = l(\mathbf{v}) \quad \forall \mathbf{v} \in \mathscr{V} \\ & \mathbb{C} \in \mathbf{C} \quad \mathbf{s} \in \mathscr{S} \end{cases} \tag{23}$$

The formulation above is an optimization problem with a convex quadratic objective functional and linear constraints, i.e. a convex quadratic programming problem. This enables to use efficient algorithms for convex quadratic programming as in the case of the formulation FR. Comments about its relation with formulations FU and FR will be made later. It will be shown that this formulation provides solutions which are similar to those given by the other formulations described.

2.3 Material Identification Problem: discrete formulations

From now on we establish an hypothesis about the constitutive model assumed for the solid. We will assume that the material is isotropic and that the Poisson ratio ν is known, therefore the constitutive tensor field can be written as $\mathbb{C}(\mathbf{x}) = E(\mathbf{x})\mathbb{C}_1$ for any point $\mathbf{x} \in \Omega$, being $\mathbb{C}_1$ the constitutive tensor corresponding to a material with unitary Young modulus. The

inverse problem now consists of finding the Young modulus scalar field $E : \Omega \to \mathbb{R}^+$. This hypothesis is valid in many MIP applications, and was applied in recent numerical studies of mechanical properties characterization in carotid arteries [18, 19].

In order to obtain numerical solutions of the optimization problems it is necessary to apply a discretization procedure to define unknowns in a finite-dimensional space. We will apply the FEM and discretize the domain using n_E triangular elements with linear interpolation functions. The Young modulus is approximated by a constant function within each element, thus the Young scalar function E is defined by a vector $\mathbf{E}$ with n_E entries. Admissible intervals are considered for the Young modulus values as in [11], which define the following entry-by-entry inequalities $\mathbf{E}_{\min} \leq \mathbf{E} \leq \mathbf{E}_{\max}$.

The FEM equation for the LEP is:

$$\mathbf{K}(\mathbf{E})\mathbf{U} = \mathbf{F} \tag{24}$$

where $\mathbf{K}(\mathbf{E})$ is the stiffness matrix of the structure, $\mathbf{F}$ is the vector of external equivalent nodal loads and $\mathbf{U}$ is the vector of nodal displacements. From now on $\mathbf{U}(\mathbf{E})$ will denote the (unique) solution of the linear system of Equation (24) for the mechanical properties $\mathbf{E}$. The stiffness matrix depends linearly on $\mathbf{E}$ by:

$$\mathbf{K}(\mathbf{E}) = \sum_{i=1}^{n_E} E_i \mathbf{K}_i \tag{25}$$

where $\mathbf{K}_i$ is the stiffness matrix of the i-th element for unitary Young modulus. For ease of notation the element matrices are in their *extended form*, i.e., $\mathbf{K}_i$ is obtained by assembling the usual element matrix in a larger null matrix.

2.3.1 Formulation NPQED

Applying the FEM to the functional of Equation (13) the following formulation is obtained:

$$\text{(NPQED)} \begin{cases} \min\limits_{\mathbf{E}} & \dfrac{1}{2} \|\mathbf{U}(\mathbf{E}) - \mathbf{U}^m\|^2_{\mathbf{M_u}} \\ \text{s.t.} & \\ & \mathbf{E}_{\min} \leq \mathbf{E} \leq \mathbf{E}_{\max} \end{cases} \tag{26}$$

where $\mathbf{M_u}$ is a positive definite symmetric matrix, $\mathbf{U}^m$ is the vector of measured nodal displacements and the norm $\|\cdot\|_{\mathbf{M_u}}$ is defined as:

$$\|\mathbf{U}\|_{\mathbf{M_u}} = \sqrt{\mathbf{U}^{\mathrm{T}}\mathbf{M_u}\mathbf{U}} \qquad \mathbf{U} \in \mathbb{R}^{n_U}. \tag{27}$$

Since $\mathbf{U}(\mathbf{E})$ is a nonlinear nonconvex function of $\mathbf{E}$, the objective functional is nonlinear as well, thus a general algorithm for nonlinear nonconvex optimization (nonlinear programming) problems must be used. That is why this formulation will be called Nonlin-

ear Programming Quadratic Error in Displacement (NPQED). The gradient of the functional can be easily calculated, therefore gradient-based algorithms should be used and eventually the Hessian matrix can be calculated for convergence improvement. However, this formulation does not fully exploit the sparse structure of $\mathbf{K}(\mathbf{E})$ so that the time needed for the identification procedure tends to be high and depends strongly on the initial point used.

Note that NPQED would be obtained if the norm $\|\cdot\|_{\mathbf{M_u}}$ is considered in the formulation FU or if the norm $\|\cdot\|_{\mathbf{K}(\mathbf{E})^{-1}\mathbf{M_u}\mathbf{K}(\mathbf{E})^{-1}}$ is used in the formulation FR, although the positive features of FR are lost.

2.3.2 Formulation NPCEG

Let us consider the formulation CEGM given by Equation (21). In order to eliminate the stress tensor as a variable we apply a procedure suggested in [36] which consists of assuming that the stress field $\boldsymbol{\sigma}$ derives from a certain displacement field $\mathbf{w}$, i.e. $\boldsymbol{\sigma} = \mathbb{C}[\boldsymbol{\varepsilon}(\mathbf{w})]$. By applying the FEM discretization we obtain:

$$\begin{cases} \min\limits_{\mathbf{E},\mathbf{W}} & \dfrac{1}{2}\|\mathbf{W}-\mathbf{U}^m\|^2_{\mathbf{K}(\mathbf{E})} \\ \text{s.t.} & \\ & \mathbf{K}(\mathbf{E})\mathbf{W} = \mathbf{F} \\ & \mathbf{E}_{\min} \leq \mathbf{E} \leq \mathbf{E}_{\max} \\ & \mathbf{W} \in \mathbb{R}^{n_U} \end{cases} \tag{28}$$

Finally we can use the constraint to eliminate the variable $\mathbf{W}$ to obtain:

$$(\text{NPCEG}) \begin{cases} \min\limits_{\mathbf{E}} & \dfrac{1}{2}\|\mathbf{U}(\mathbf{E})-\mathbf{U}^m\|^2_{\mathbf{K}(\mathbf{E})} \\ \text{s.t.} & \\ & \mathbf{E}_{\min} \leq \mathbf{E} \leq \mathbf{E}_{\max} \end{cases} \tag{29}$$

As in the formulation NPQED, a general nonlinear programming algorithm must be applied to solve this formulation and that is why this formulation is called Nonlinear Programming Constitutive Equation Gap (NPCEG). Although the functional is nonlinear, it is convex, hence each local minimum is a global solutions of the optimization problem. This property is very important, particularly when gradient-based algorithms are used, as it is done in many articles in the literature [17,18,19]. This formulation will be solved using a gradient-based algorithm.

It is seen that NPCEG would be obtained if the norm $\|\cdot\|_{\mathbf{K}(\mathbf{E})}$ is used in the formulation FU, or if the norm $\|\cdot\|_{\mathbf{K}(\mathbf{E})^{-1}}$ is used in the formulation FR. Once again, the positive features of FR are lost.

2.3.3 Formulation CPCEG

In this section we introduce a new formulation that presents strong advantages in computational efficiency compared to the ones described above. The formulation consists of a Conic Programming problem and it was not seen by the authors in the literature.

Let us consider the functional of the formulation NPCEG. Using that $\mathbf{K}(\mathbf{E})\mathbf{U}(\mathbf{E}) = \mathbf{F}$ with $\mathbf{K}(\mathbf{E})$ symmetric, we have

$$\frac{1}{2}\left\|\mathbf{U}(\mathbf{E}) - \mathbf{U}^m\right\|^2_{\mathbf{K}(\mathbf{E})} = \frac{1}{2}\mathbf{F}^{\mathrm{T}}\mathbf{K}^{-1}(\mathbf{E})\mathbf{F} - (\mathbf{U}^m)^{\mathrm{T}}\mathbf{F} + \frac{1}{2}(\mathbf{U}^m)^{\mathrm{T}}\mathbf{K}(\mathbf{E})\mathbf{U}^m. \tag{30}$$

Since $(\mathbf{U}^m)^{\mathrm{T}}\mathbf{F}$ does not depend on $\mathbf{E}$, the NPCEG can be expressed as:

$$\begin{cases} \min\limits_{\mathbf{E}} & \frac{1}{2}(\mathbf{U}^m)^{\mathrm{T}}\mathbf{K}(\mathbf{E})\mathbf{U}^m + \frac{1}{2}\mathbf{F}^{\mathrm{T}}\mathbf{K}^{-1}(\mathbf{E})\mathbf{F} \\ \text{s.t.} & \\ & \mathbf{E}_{\min} \leq \mathbf{E} \leq \mathbf{E}_{\max} \end{cases} \tag{31}$$

The problem above can be expressed equivalently as:

$$\begin{cases} \min\limits_{\mathbf{E},\tau_U,\tau_F} & \frac{1}{2}\tau_U + \frac{1}{2}\tau_F \\ \text{s.t.} & \\ & (\mathbf{U}^m)^{\mathrm{T}}\,\mathbf{K}(\mathbf{E})\,\mathbf{U}^m \leq \tau_U \\ & \mathbf{F}^{\mathrm{T}}\,\mathbf{K}(\mathbf{E})^{-1}\,\mathbf{F} \leq \tau_F \\ & \mathbf{E}_{\min} \leq \mathbf{E} \leq \mathbf{E}_{\max} \end{cases} \tag{32}$$

The stiffness matrix can be written in the following way:

$$\mathbf{K}(\mathbf{E}) = \sum_{i=1}^{n_E} E_i\,\mathbf{B}_i^{\mathrm{T}}\mathbb{C}_1\mathbf{B}_i\,\Omega_i\,t = \sum_{i=1}^{n_E} E_i\,\tilde{\mathbf{B}}_i^{\mathrm{T}}\,\tilde{\mathbf{B}}_i \tag{33}$$

where $\mathbf{B}_i$ is the matrix of interpolation function derivatives of the i-th element in its extended form, and $\tilde{\mathbf{B}}_i^{\mathrm{T}} = \sqrt{\Omega_i t}\,\mathbf{B}_i^{\mathrm{T}}\mathbb{C}_1^{\frac{1}{2}}$, t is the thickness of the solid and Ω_i is the area of the i-th element. Using the procedure described in [7] the nonlinear constraint $\mathbf{F}^{\mathrm{T}}\,\mathbf{K}(\mathbf{E})^{-1}\,\mathbf{F} \leq \tau_F$ is replaced by a set of linear constraints and a set of second-order cone constraints. The final formulation has the following expression:

$$(\text{CPCEG}) \begin{cases} \min\limits_{\mathbf{E},\tau_U,\tau_F,\mathbf{e},\tilde{\boldsymbol{\sigma}}} & \frac{1}{2}\tau_U + \frac{1}{2}\tau_F \\ \text{s.t.} & \\ & (\mathbf{U}^m)^{\mathrm{T}}\,\mathbf{K}(\mathbf{E})\,\mathbf{U}^m \leq \tau_U \\ & \sum_{i=1}^{n_E} e_i \leq \tau_F \\ & \sum_{i=1}^{n_E} \tilde{\mathbf{B}}_i^{\mathrm{T}}\,\tilde{\boldsymbol{\sigma}}_i = \mathbf{F} \\ & \|\tilde{\boldsymbol{\sigma}}_i\|^2 \leq E_i\,e_i \quad i = 1,\ldots,n_E \\ & \mathbf{E}_{\min} \leq \mathbf{E} \leq \mathbf{E}_{\max} \end{cases} \tag{34}$$

where $\mathbf{e} = (e_1, \ldots, e_{n_E}) \in \mathbb{R}^{n_E}$ and $\tilde{\boldsymbol{\sigma}}_i \in \mathbb{R}^{3n_E}$ with $(i = 1, \ldots, n_E)$ are auxiliary variables. At the solution, the vector $\tilde{\boldsymbol{\sigma}}_i$ is directly related with the statically admissible stress, i.e., $\boldsymbol{\sigma} = \sqrt{\Omega t}\,\mathbb{C}_1^{\frac{1}{2}}\tilde{\boldsymbol{\sigma}}$. The vectors are presented in the extended form. The tensor field $\boldsymbol{\sigma}$ is the stress obtained when the LEP is solved using the solution mechanical parameters. Let us remark that this formulation can also be obtained from Equation (21).

The formulation obtained is a second-order cone programming problem. We will call this formulation Conic Programming Constitutive Equation Gap (CPCEG). There exist efficient algorithms for the resolution of this kind of problems [8]. Moreover, since the obtained formulation is equivalent to the NPCEG, it inherits the listed positive theoretical properties.

2.3.4 Formulation QPCEG

In this section we apply the discretization to the formulation given by Equation (23). The tensor field $\mathbf{s}$ leads to an internal auxiliary stress vector $\mathbf{S} \in \mathbb{R}^{3n_E}$, and $\mathbf{S}_i$ is a vector with the respective entries of the i-th element. The following equality is obtained for isotropic material with constant Poisson ratio:

$$\frac{1}{2}\int_\Omega \mathbf{s} : (\mathbb{C}^{(k)})^{-1}[\mathbf{s}]\,\mathrm{d}V = \sum_{i=1}^{n_E} \frac{1}{E_i^{(k)}} (\mathbf{S}_i)^{\mathrm{T}} \mathbb{C}_1^{-1} (\mathbf{S}_i) \Omega_i t. \tag{35}$$

To simplify the notation, let us define the matrix $\mathbf{M}^{(k)}$

$$\mathbf{M}^{(k)} = \begin{bmatrix} \mathbf{M}_1^{(k)} & 0 & \ldots & 0 \\ 0 & \ddots & \ddots & \vdots \\ \vdots & \ddots & \ddots & 0 \\ 0 & \ldots & 0 & \mathbf{M}_{n_E}^{(k)} \end{bmatrix} \qquad \mathbf{M}_i^{(k)} = \frac{t\Omega_i}{E_i^{(k)}} \mathbb{C}_1^{-1} \tag{36}$$

Using these expressions and applying the discretization to Equation (23) we obtain:

$$(\text{QPCEG}) \begin{cases} \min\limits_{\mathbf{E},\mathbf{S}} & \frac{1}{2}\mathbf{S}^{\mathrm{T}}\mathbf{M}^{(k)}\mathbf{S} \\ \text{s.t.} & \\ & \mathbf{K}(\mathbf{E})\,\mathbf{U}^m + \mathbf{B}^{\mathrm{T}}\mathbf{S} = \mathbf{F} \\ & \mathbf{E}_{\min} \leq \mathbf{E} \leq \mathbf{E}_{\max} \\ & \mathbf{E} \in \mathbb{R}^{n_E}, \quad \mathbf{S} \in \mathbb{R}^{3n_E} \end{cases} \tag{37}$$

where $\mathbf{B}$ is the assemble matrix of the derivatives of the interpolation functions $\mathbf{B}^T = \left[\mathbf{B}_1^T \ldots \mathbf{B}_{n_E}^T\right]$.

The optimization problem has a convex quadratic objective functional, n_U linear constraints, $2n_E$ box constraints and $4n_E$ variables, thus it is a convex quadratic programming optimization problem, and we call the formulation Quadratic Programming Constitutive Equation Gap (QPCEG). This enables us to use efficient quadratic programming algorithms,

as in the formulation FR, maintaining the convexity feature. It will be seen that this formulation is appropriate for the application of regularization techniques.

2.4 Regularization term

Since experimental measurements always have error, every identification formulation needs the application of certain regularization technique. The application of regularization techniques reduces the numerical instability of the solution of an ill-posed problem. In order to use these techniques some information or assumption about the real material distribution must be considered. One of the most used approaches, specially when optimization formulations are used, is the addition of a *regularization term* to the objective functional [40]:

$$\mathscr{F}_\alpha(E) = \mathscr{J}(E) + \alpha \mathscr{R}(E) \tag{38}$$

where $\mathscr{R}(E)$ is the regularization term, which depends on the unknown field, and α is a regularization factor that controls how much the solution is regularized.

In the MIP formulations considered in this article the Total Variation (TV) regularization will be considered:

$$\mathscr{R}(E) = \|\nabla E\|_{L_1(\Omega)^2} = \int_\Omega |\nabla E| \, \mathrm{d}\Omega. \tag{39}$$

This functional penalizes distributions presenting high gradients in Ω, such as highly oscillating distributions. However, this functional does not penalizes excessively high gradients concentrated in sets of zero measure, such as surfaces or curves. Therefore the TV is considered appropriate when the solutions are expected to be piecewise smooth distributions [40].

One important disadvantage of the TV is that it is a non-differentiable function of E. This feature may impede the use of gradient-based optimization algorithms. To avoid this issue, in [40] Vogel recommends the use of the modified term $\| \sqrt{|\nabla E|^2 + \beta^2} \|_{L_1(\Omega)}$ instead of $\mathscr{R}$, where β is a real parameter. The requirement of an additional parameter β, which requires an effective tuning strategy, represents a disadvantage of the methodology, however it can be applied as in [22, 23]. In this paper an equivalent differentiable form the discrete version of the optimization problem is used, hence the original TV is used and the parameter β is not needed.

If the finite element mesh contains n_{seg} interior segments, where each one separates two elements, it can be easily shown that the TV of Equation (39), can be computed as:

$$\mathscr{R}(\mathbf{E}) = \sum_{m=1}^{n_{seg}} |\mathbf{P}_m \mathbf{E}| = \|\mathbf{P}\mathbf{E}\|_1 \tag{40}$$

where $\mathbf{P}$ is a $n_{seg} \times n_E$ matrix having $\mathbf{P}_m$ as its m-th row. If the segment m separates the elements p and q, with $p < q$, the matrix $\mathbf{P}$ is given by:

$$\mathbf{P}_{mj} = \begin{cases} \ell_m & \text{if } j = p \\ -\ell_m & \text{if } j = q \\ 0 & \text{if } j \neq q \text{ and } j \neq p \end{cases} \tag{41}$$

where ℓ_m is the length of the segment m.

This regularization term is nonlinear and non-differentiable thus the following equivalence is considered:

$$\|\mathbf{PE}\|_1 \quad \equiv \quad \begin{cases} \min\limits_{\mathbf{Z}} & \mathbf{1}_{n_{seg}}^{\mathrm{T}} \mathbf{Z} \\ \text{s.t.} & \\ & \mathbf{PE} - \mathbf{Z} \leq 0 \\ & -\mathbf{PE} - \mathbf{Z} \leq 0 \\ & \mathbf{Z} \in \mathbb{R}^{n_{seg}} \end{cases} \tag{42}$$

where $\mathbf{1}_{n_{seg}}^{\mathrm{T}} = (1, \ldots, 1) \in \mathbb{R}^{n_{seg}}$. Using the expression presented above, an optimization problem defined by differentiable functions is obtained.

2.4.1 Regularization factor analysis

One of the most important aspects of the regularization technique is the selection of the regularization factor α. In this article the Morozov criterion is considered for the selection of α [40], as it is done in some examples of the literature [22]. In this methodology it is established that α should be the largest value such that $M(\alpha) \leq M_{obj}$, where $M(\alpha)$ is the Morozov coefficient defined as:

$$M(\alpha) = \frac{\|\mathbf{u}_\alpha^* - \mathbf{u}^m\|_{L_2(\Omega)^2}}{\delta_e}, \tag{43}$$

where δ_e is an estimated error level and $\mathbf{u}_\alpha^*$ is the displacement field obtained using the solution of the MIP with the regularization factor α. In real life problems the error level δ_e should be defined taking into account the precision of the instruments, the error level introduced by the image processing methods used to obtain $\mathbf{u}^m$, etc. In the examples solved in this article we set

$$\delta_e = \beta \, \|\mathbf{u}^r - \mathbf{u}^m\|_{L_2(\Omega)^2} \, . \tag{44}$$

For the automatic selection of α the bisection method in a logarithmic scale was applied. The target Morozov parameter $M_{obj} = 0.95$ should be reached within the tolerance 0.05. Note that the bisection method implies an iteration where each step requires the complete solution of one optimization problem.

3 Numerical Results

In order to compare the performance of the described formulations, in this section we solve four numerical examples. The problems are similar to the most used in the recent material identification literature. In all the numerical examples solved, errors are introduced in the data in order to avoid committing an *inverse crime* [24].

About the software used To solve the optimization problems of the formulations NPQED and NPCEG the MATLAB *fmincon* function is used with the following options: Algorithm: interior-point, TolFun: 10^{-9} , TolX: 10^{-9}. Function derivatives provided to *fmincon* are computed by evaluating the analytical expressions. The second order cone programming problem CPCEG is solved using Sedumi v1.30 [39] in MATLAB. The formulation QPCEG is solved using the MATLAB function *quadprog*. For the elasticity problem a FEM code implemented by the first author was used, using GMSH as mesh generator [20] and Paraview for the visualization [4]. All the examples were solved using an Intel Core i7, 8 GB RAM computer. The optimization algorithms always succeeded to obtain a solution satisfying the stopping criteria, unless otherwise indicated.

Error measurements To measure the error of the obtained solutions in each example we use different norms of the relative error Δ_E and the norms $L_1(\Omega)$ and $L_2(\Omega)$ as follows:

$$\delta E_{L_p} = \frac{\|\Delta_E\|_{L_p(\Omega)}}{\|1\|_{L_p(\Omega)}} \qquad p = 1,2 \qquad \Delta_E = \frac{|E^* - E^r|}{E^r} \tag{45}$$

where E^r is the reference or solution Young modulus field and E^* is the Young modulus obtained using the identification method. We will also use the sup norm as follows:

$$\delta E_\infty = \frac{\|\Delta_E\|_{L_\infty(\Omega)}}{\|1\|_{L_\infty(\Omega)}} = \sup_{x\in\Omega} \Delta_E. \tag{46}$$

3.1 Example 1

The aim of this example is to obtain a first performance comparison of the formulations described. This is done through the resolution of a reference problem widely used in the literature [17,31,34]. In particular we are interested in the numerical confirmation of the equivalence between the formulations CPCEG and NPCEG, and the evaluation of the effectiveness of the TV-based regularization technique with the proposed formulations.

The problem consists of a solid occupying a square region with side $\ell = 0.01$ m and unitary thickness, formed by a linear elastic material and submitted to a plane strain state. The Poisson ratio is $\nu = 0.3$ and the Young modulus is defined in two regions as it is seen in Figure 2, with the reference values $E_1^r = 1$ MPa and $E_2^r = 2$ MPa. The applied load is

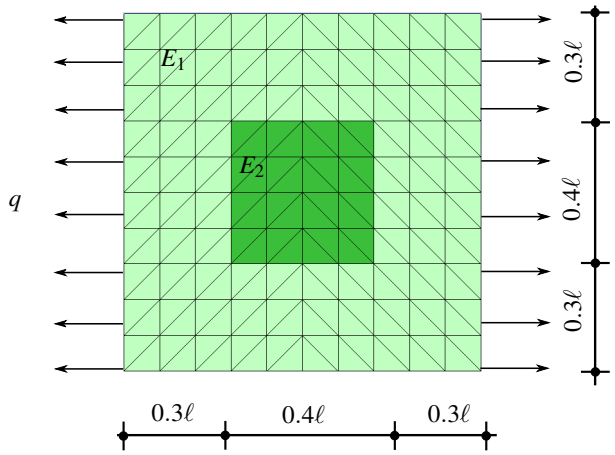

Fig. 2 Example 1 geometry, boundary conditions and mesh with 200 elements.

$q = 1$ MPa. In the articles cited, this example is used to perform identification of Poisson and Young parameters, but no regularization is applied. In this case we will identify the Young modulus only and apply the described regularization technique to reduce the effect of the data error over the solution obtained.

In order to emulate the experimentally measured displacements error is added to the reference displacements as it is done in numerous articles in the literature. In this example two different sets of synthetic data will be used, considering two different sources of error: random error in the reference Young modulus and error produced by interpolation of the displacements between different meshes. A justification for the mesh interpolation error is presented later.

Since one of the goals is to compare the formulations NPQED and NPCEG, the same stopping criterion parameters shall be used. In both formulations the functional is scaled using the norm of the functional gradient at the initial point. The initial point is the uniform distribution $E(x) = 1.5$ MPa. The identification for $\alpha^{(k+1)}$ is done using as initial point the Young modulus values obtained as solution using $\alpha^{(k)}$. For the formulation CPCEG no initial point is provided (the algorithm does not require it) and the options used for the Sedumi are `pars.eps=0` and `pars.bigeps=`10^{-30}. The formulation QPCEG is solved with the `quadprog` MATLAB function. It does not require an initial point, but the uniform value $E(x) = 1.5$ MPa was used as $\mathbf{E}^{(k)}$ in the functional of Equation (37). In the case of the formulation QPCEG the E^* obtained for each α value is used as $\mathbf{E}^{(k)}$ for the identification using the next α defined by the strategy used for the α selection. For the initialization of the bisection process it is considered the initial interval $[\alpha_{left}, \alpha_{right}]$ with $\alpha_{left} = 10^{-40}$ and $\alpha_{right} = 10^{5}$.

3.1.1 Results for random error in E

In this case the error is obtained by introducing random error in the reference Young modulus, this methodology is similar to the procedure applied in [10].

The reference Young modulus and the structured mesh of 200 linear triangular elements shown in Figure 2 are used to solve the direct problem and to generate the reference displacements $\mathbf{U}^r$. The reference displacements are shown in Figure 3. Then, errors are added

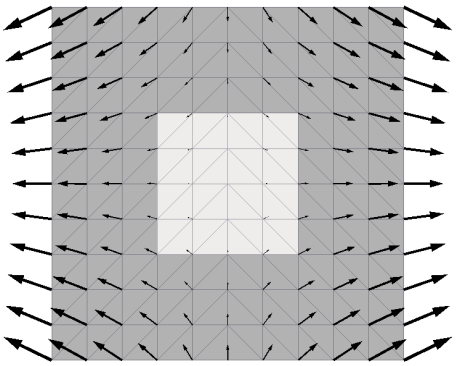

Fig. 3 Example 1 reference displacements, scale factor 0.3.

to the reference material parameters $\mathbf{E}^r$ obtaining noisy parameters $\mathbf{E}^m$, which are used to calculate the measured displacements $\mathbf{U}^m$ by solving the direct problem with the same mesh of 200 elements.

The Young reference value of each element E_i^r is modified adding a normal distributed random value d_{E_i} as follows:

$$E_i^m = E_i^r(1+d_{E_i}) \qquad i=1,\ldots,n_E \tag{47}$$

where the standard deviation is set such that the introduced error level η_E is independent of the mesh. The E error level η_E is defined as follows:

$$\eta_E = \frac{\|d_E\|_{L_1(\Omega)}}{\|1\|_{L_1(\Omega)}} = \frac{\left\| \frac{|E^m-E^r|}{E^r} \right\|_{L_1(\Omega)}}{|\Omega|}, \tag{48}$$

where $|\Omega|$ represents the area of the domain Ω.

If all the elements have approximately the same area, then the quantity $d_{E_i}|\Omega_i|$ can be considered as a normal distributed random variable $X \sim \mathcal{N}(0,\sigma_E^2)$. Substituting this in the definition of η_E and using the properties of the expected value, it can be shown that the

standard deviation should be

$$\sigma_E = \eta_E \sqrt{\frac{\pi}{2}} \frac{|\Omega|}{n_E}, \tag{49}$$

in order to obtain a Young modulus distribution with error level η_E.

The displacements $\mathbf{U}^m$ are obtained solving the direct problem using the material parameters $\mathbf{E}^m$. Three levels of error are considered: $\eta_E = 0.01$, 0.05 and 0.1.

To select the regularization parameter α, the procedure described in the Section 2.4.1 is applied for all the formulations using $\beta = 1$ in Equation (44). Table 1 presents the results obtained for the different error levels η_E. In the table CPCEGNR means CPCEG without

Form	$\eta_E = 0.01$			$\eta_E = 0.05$			$\eta_E = 0.1$		
	δE_{L_1}	δE_∞	time (s)	δE_{L_1}	δE_∞	time (s)	δE_{L_1}	δE_∞	time (s)
NPQED	1.096	19.544	23252.9	3.753	39.662	19992.7	6.373	37.996	18643.0
NPCEG	0.510	5.139	15067.0	2.485	14.556	14676.6	4.737	27.488	12740.0
CPCEG	0.510	5.096	29.4	2.485	14.501	27.4	4.737	27.486	24.4
QPCEG	0.525	6.120	7.6	2.321	15.920	8.2	4.511	29.913	7.7
CPCEGNR	1.344	5.906	2.7	4.530	16.959	2.8	10.289	48.388	2.7

Table 1 Example 1 results for synthetic data obtained applying error in E.

regularization ($\alpha = 0$) and 'time' means the total time required to obtain the final solution.

The first important observation is that the results obtained by the formulations NPCEG and CPCEG are almost identical in the error, confirming that these formulations are equivalent. However the CPCEG requires nearly 500 times less time than NPCEG, which represents an important advantage. It can also be seen that the formulation NPQED requires a time 40% higher than that of NPCEG, obtaining a slightly higher error in E. Finally we see that the formulation QPCEG provides, in this case, results which are comparable to those given by NPCEG and CPCEG. Moreover, the time required by QPCEG is a third of the time needed by the formulation CPCEG.

3.1.2 Results for interpolation error in $\mathbf{U}$

In this case the data with error is obtained through the interpolation between different meshes. This kind of error can be present in real life problems when the data displacements are measured in a set of points different to the nodes of the FEM mesh used for the resolution of the inverse problem as in [18].

The reference displacements are generated using the reference Young modulus and the structured mesh with 20000 elements. After that, those displacements are interpolated to the mesh with 200 elements used in the previous section. This interpolation introduces an error

level $\eta_{\mathbf{u}} = 1.77\%$, where the error level is given by:

$$\eta_{\mathbf{u}} = \frac{\|\mathbf{u}^m - \mathbf{u}^r\|_{L_2(\Omega)^2}}{\|\mathbf{u}^r\|_{L_2(\Omega)^2}}. \tag{50}$$

The error levels $\eta_{\mathbf{u}}$ obtained in the previous section were $\eta_{\mathbf{U}} = 0.27\%$, 0.94% and 2.4% which correspond to $\eta_E = 0.01$, 0.05 and 0.1 respectively. However it is important to remark that this error has a different nature. Given $\mathbf{U}^m$ with interpolation error, it may not exist any field E solving exactly the inverse problem.

In Table 2 we see the error of the solutions obtained as well as the times required for the identifications. In the table 'time' means the total time required to obtain the final solution,

Form	δE_{L_1}	δE_∞	α	$M(\alpha)$	time(s)	its	time/its (s)
NPQED	5.613	40.59	2.690	0.957	24115	7	3445
NPCEG	0.747	3.811	20.35	0.962	15622	8	1953
CPCEG	0.747	3.811	20.35	0.962	21	8	2.7
QPCEG	0.559	3.386	4.5×10^{-12}	0.916	7	8	0.9
CPCEGNR	39.32	110.4	0	-	2.8	1	2.8

Table 2 Example 1 results for synthetic data obtained applying error in **U**.

'its' represents the number of iterations required by the bisection method, hence the value 'time/its' indicates the average time required by each formulation to perform the identification for a given value of α. The values α and $M(\alpha)$ correspond to the last iteration of the bisection method.

We note that the formulation NPQED requires a time considerably higher than the other formulations, and provides a solution with a higher error. The formulation NPCEG achieves a solution with lower error in less time that NPQED, and this will be our reference formulation. The formulation CPCEG provides results which are identical to that of NPCEG in nearly 1000 times less time. The formulation QPCEG obtained a solution with lower error than the other formulations in one third of the time required by CPCEG.

To see the results graphically we present plots of mechanical properties (blue color scale) and relative error maps (red-yellow color scale). In Figure 4 we start with the mechanical properties and relative error plots obtained when the identification is performed without regularization (CPCEGNR) using the data with error in **U**.

The plots presented in Figure 5 represent the mechanical properties obtained when the four formulations are applied using data with error introduced in **U**. In Figure 6 the plots of the respective Young modulus relative error can be seen.

Looking at the results obtained for the formulations NPCEG and CPCEG we confirm what was expected: both formulations are equivalent, and that is why they provide almost

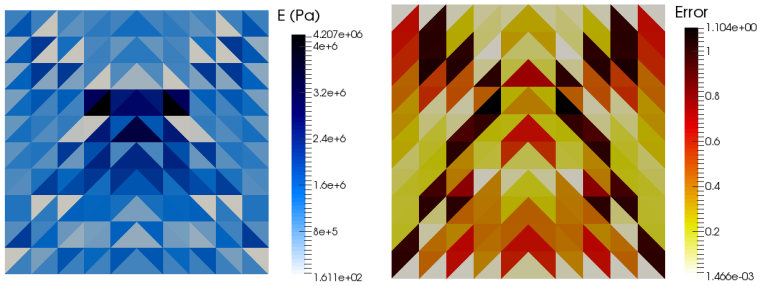

(a) Properties CPCEGNR (b) Errors CPCEGNR

Fig. 4 Example 1 results obtained without regularization for synthetic data obtained applying error in **U**.

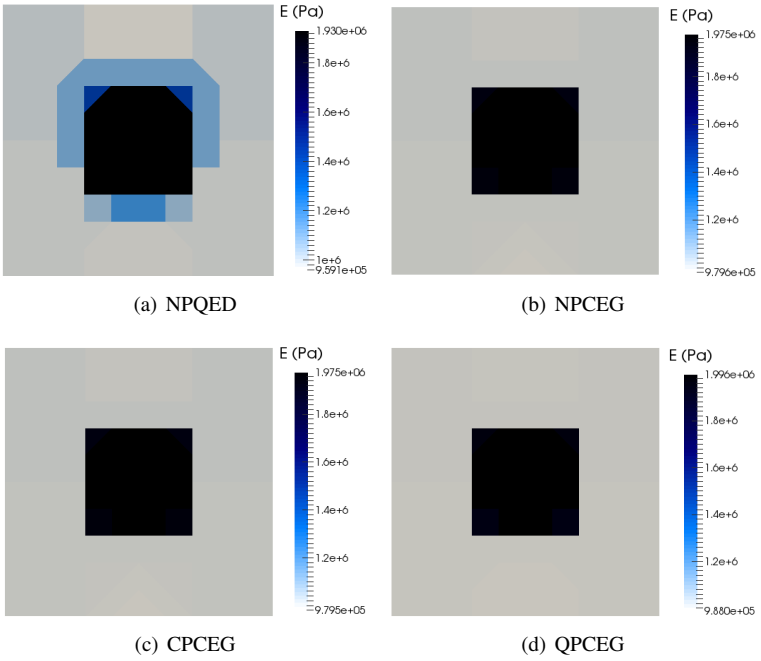

(a) NPQED (b) NPCEG

(c) CPCEG (d) QPCEG

Fig. 5 Example 1 Young modulus results for synthetic data obtained applying error in **U**.

identical Young modulus distributions. However, we see that the formulation CPCEG is more efficient, since it requires a considerably lower time. This is why we will not use the formulation NPCEG in the following examples, as well as for the formulation NPQED. We also note that in this example, the formulation QPCEG presents results as good as those obtained by the formulation CPCEG, and lower times were required. Analyzing the results obtained when no regularization is used, we conclude that it is needed to add a regularization term to improve the quality of the E distributions obtained.

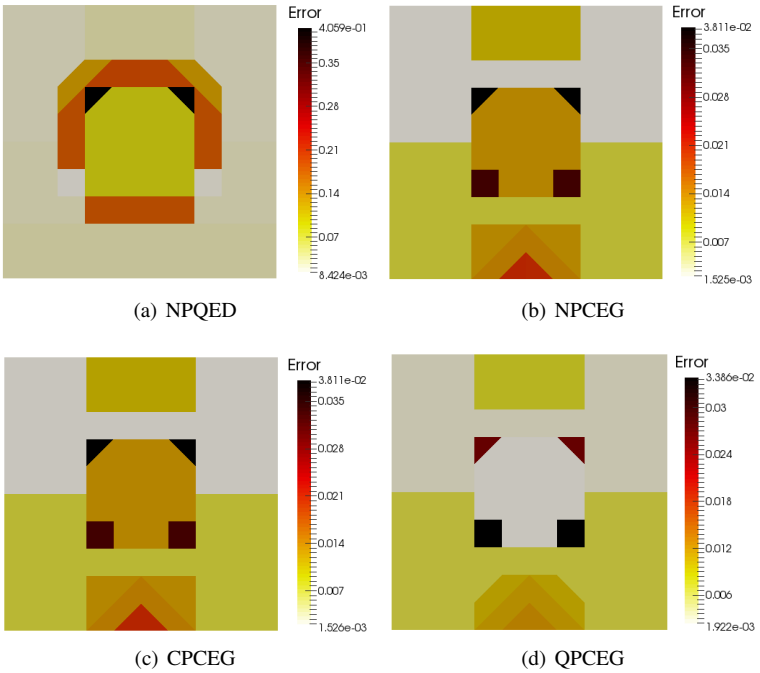

(a) NPQED (b) NPCEG

(c) CPCEG (d) QPCEG

Fig. 6 Example 1 Young modulus relative errors results for synthetic data obtained applying error in **U**.

3.2 Example 2

This example is considered to obtain a more complete performance comparison between the formulations CPCEG and QPCEG. The geometry considered in this case also corresponds to a problem usually used in the literature [5]. We start by describing the problem, and after that, we present the results obtained when different kinds of errors are introduced in the data.

The geometry of the problem consists of a square domain with side of length $\ell = 0.1$ m with two circular inclusions with radius 0.0125 m and boundary conditions seen in Figure 7. The reference Young modulus considered are: $E_1^r = 2.5$ MPa, $E_2^r = 10$ MPa and $E_3^r = 5$ MPa. The material is assumed linear elastic and isotropic with known uniform Poisson ratio $\nu = 0.2$. A displacement field is generated by solving the direct problem with an applied load $q = 1$ Mpa.

3.2.1 Results for random error in E

We start introducing error in the Young modulus in the same fashion as it was done in Section 3.1.1, using $\eta_E = 0.1$. As it was done in the previous example, the bound values for E considered are $E_{\min} = 10$ Pa and $E_{\max} = 10^9$ Pa. The stopping criterion used for the algorithms are the same as in the previous example. An unstructured mesh with 1078

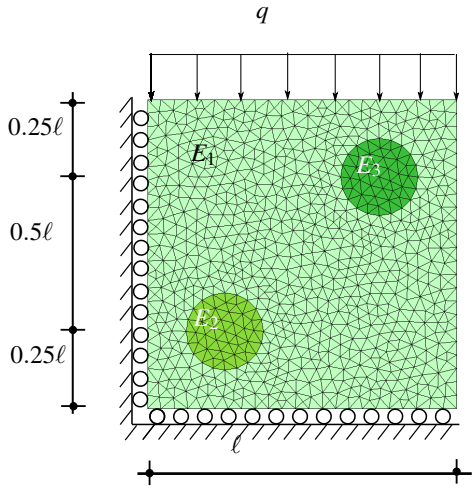

Fig. 7 Example 2 geometry, boundary conditions and mesh with 1552 elements.

triangular elements is used for the generation of the displacements and the identification procedure. The selection of the α is done automatically using the methodology described in Section 2.4.1, with $\alpha_{left} = 10^{-40}$ and $\alpha_{right} = 10^{5}$.

In Table 3 we see the results obtained when the formulations CPCEG and QPCEG are applied. We see that the Young modulus distributions obtained by both formulations present

Form	δE_{L_1}	δE_{∞}	time(s)	its	time/its (s)
CPCEG	3.705	23.405	667.5	8	83.4
QPCEG	3.612	23.819	53.0	9	5.9

Table 3 Example 2 results, error in E, $\eta_E = 0.1$.

similar errors, while the formulation QPCEG requires less than a tenth of the time needed by the CPCEG.

Let us see the results graphically, in Figure 8 the Young modulus values obtained are presented. We can see that both formulations successfully identify the geometry of the inclusions, however there exists a notorious error in the Young modulus value in one of the inclusions. This can be seen more clearly in Figure 9 which shows the relative error plots obtained with each formulation. In these images we can see that in region 2 both formulations obtain solutions with 23% of relative error, while in region 3, the CPCEG produces a slightly lower error than the QPCEG. However we conclude that for this example both formulations allow a correct identification, being the formulation QPCEG remarkably more efficient than CPCEG.

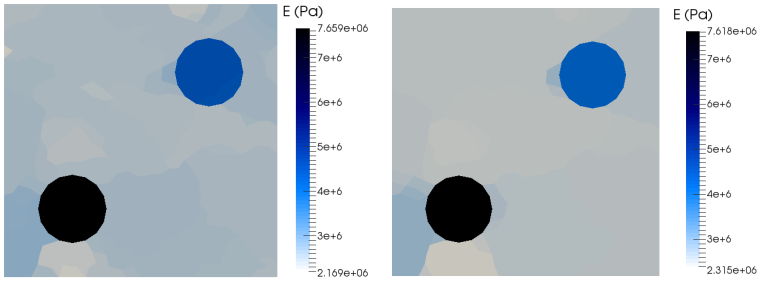

(a) CPCEG (b) QPCEG

Fig. 8 Example 2 Young modulus results for synthetic data obtained applying error in E.

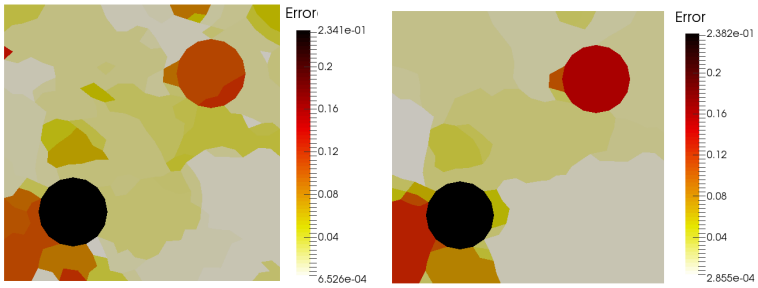

(a) CPCEG (b) QPCEG

Fig. 9 Example 2 Young modulus relative errors results for synthetic data obtained applying error in E.

3.2.2 Results for interpolation error in **U**

In this case it is considered an error included directly in the displacements vector by using the procedure applied in [5,43]. The results obtained in this work and in the papers cited are not directly comparable since more than one displacement field is used, thus a different MIP is solved.

To produce the "measured" displacements the direct problem is solved using the reference Young modulus and an unstructured mesh with 12312 elements. The nodal displacements obtained are called reference displacements $\mathbf{U}^r$ and random error is added as follows:

$$U_i^m = U_i^r(1+\delta_U r_i) \tag{51}$$

where r_i is the i-th entry of a normal distributed random vector with zero mean and unitary variance, and $\delta_U = 0.01$. These nodal displacements are finally interpolated to the mesh used for the identification, which have a lower number of elements. In this example we will consider three meshes with $1,078$, $1,552$ and $3,186$ elements, where the final error levels η_U are: 0.59%,0.58% and 0.57%, respectively. In Figure 10 the interpolated displacements $\mathbf{U}^m$ are shown for the mesh with 1552 elements.

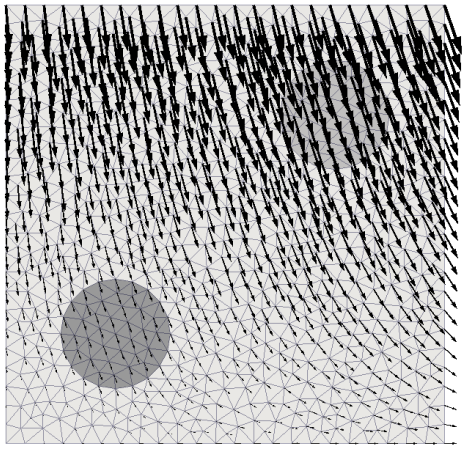

Fig. 10 Example 2 measured displacements, scale factor 0.3.

In Table 4 we see the results obtained after the identification. Once again we see that the

Form	n_E	δE_{L_1}	δE_∞	α	time(s)
CPCEG	1078	5.810	47.215	1.19×10^{-4}	91.3
QPCEG	1078	7.499	47.502	2.15×10^{-14}	7.8
CPCEG	1552	5.805	40.936	1.19×10^{-4}	249.9
QPCEG	1552	8.161	45.972	9.43×10^{-15}	9.6
QPCEG	3186	11.74	68.070	2.03×10^{-15}	23.7

Table 4 Example 2 results, error in $\mathbf{U}$, $\delta_U = 0.01$.

formulation QPCEG requires less time than CPCEG (10 times less), however in this case the error obtained by the QPCEG is 30% higher. We also see that as the mesh size increases the formulation CPCEG slightly reduces the error obtained, which does not occurs for the formulation QPCEG. The formulation CPCEG requires higher memory resources, and this is why it could not be applied for the mesh with 3186 elements. The formulation QPCEG is able to solve this large problem due to the low number of variables and the efficiency of the quadratic programming algorithms used.

In Figure 11 we see the Young modulus obtained for both formulations using the mesh with 1552 elements. Both formulations achieve an acceptable identification of the inclusions, however the formulation CPCEG provides results with higher precision.

In Figure 12 we see the relative errors obtained for both formulations using the mesh with 1552 elements.

The results seen in this example establish a first clear difference between the formulations QPCEG and CPCEG: the formulation CPCEG provides solutions with less error while QPCEG provides results with acceptable error in less time. Since the formulation CPCEG

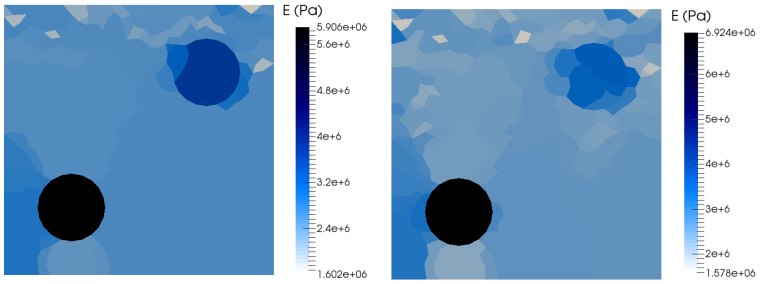

(a) CPCEG (b) QPCEG

Fig. 11 Example 2 Young modulus results for synthetic data obtained applying error in $\mathbf{U}$ with $\delta_U = 0.01$.

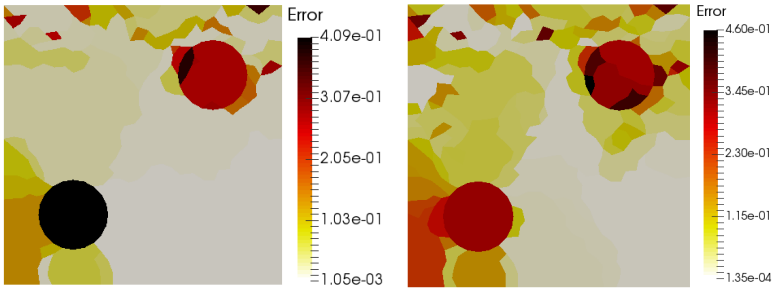

(a) CPCEG (b) QPCEG

Fig. 12 Example 2 error results for synthetic data obtained applying error in $\mathbf{U}$ with $\delta_U = 0.01$.

has shown to provide more precise results, only this formulation will be used in the following example.

3.3 Example 3

In Biomechanics applications, the direct problem involves nonlinear models, for instance in [23] a nonlinear elastic model is considered for identification of the mechanical properties of mammary tumors.

In this example we study the results obtained when the simulated measures are obtained considering the non-linearities of finite elasticity. In addition we assume that there is no information about the internal interfaces, location of inclusions, etc, therefore for the MIP resolution a structured mesh is used. In particular we study an example where the internal interfaces cannot be found as element boundaries. In this example, the formulation CPCEG is applied.

The problem considered consists of a square domain with side of length $\ell = 1$ m, with one circular inclusion of radius 0.25 m and boundary conditions shown in Figure 13. The

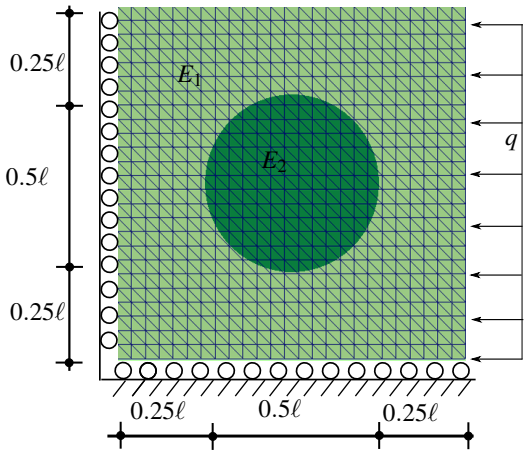

Fig. 13 Example 3 geometry, boundary conditions and mesh with 1250 elements.

hyperelastic behavior of the material is given by the Curnier model [13], thus the strain-energy function is

$$\Psi(\mathbf{L}) = \lambda(J - \log(J) - 1) + \mu \mathrm{Tr}(\mathbf{L}^2) \tag{52}$$

where $J = \det(\mathbf{I} + \nabla \mathbf{u})$, $\mathbf{L} = \frac{1}{2}(\nabla \mathbf{u} + \nabla^T \mathbf{u} + \nabla^T \mathbf{u} \nabla \mathbf{u})$ is the Lagrange deformation tensor and λ and μ are positive parameters. It can be seen that λ and μ are the Lamé parameters of the linearized constitutive model. The reference mechanical parameters are $\lambda = 20/3$ Pa and $\mu = 4$ Pa for the inclusion, while for the rest of the domain the parameters are $\lambda = 2/3$ Pa and $\mu = 0.4$ Pa. Then, if small strains are considered, the linearized model has $\nu = 0.25$ and $E = 1$ Pa for the square, and $\nu = 0.25$ and $E = 10$ Pa for the inclusion.

The applied load $q = 0.12$ Pa produces the large deformations in the solid depicted in Figure 14. The direct problem is solved using an unstructured mesh formed by 2254 triangular elements. In Figure 14 the deformed and undeformed meshes are shown, as well as the magnitude of the displacement field.

The displacements are interpolated to a regular grid of 26×26 points obtaining the measured displacements $\mathbf{U}^m$. These points of the grid define a structured mesh of 1250 elements shown in Figure 15. This mesh will be considered for the inverse problem, therefore, the inclusion interfaces are not represented by boundaries of the finite elements.

The stopping criteria considered for the SeDuMi executions are the same as in the previous examples. For the bisection process $\alpha_{left} = 10^{-10}$ and $\alpha_{right} = 10^2$ are considered, and $\beta = 1.15$ is used.

The result for $\alpha = 5.62 \times 10^{-4}$ is shown in Figure 15. The figure shows that the inclusion boundary is adequately identified. Moreover, although the measured displacements correspond to a nonlinear model, the mechanical parameters of the linearized model are correctly estimated.

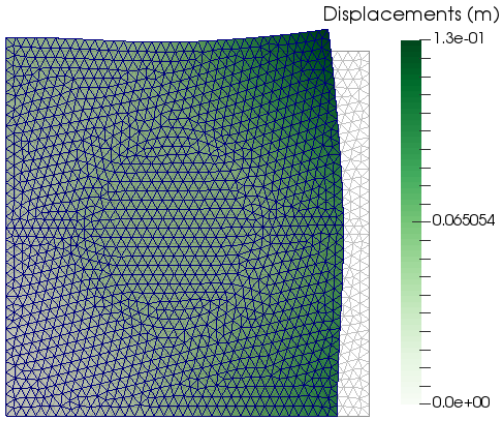

Fig. 14 Example 3 nonlinear behavior.

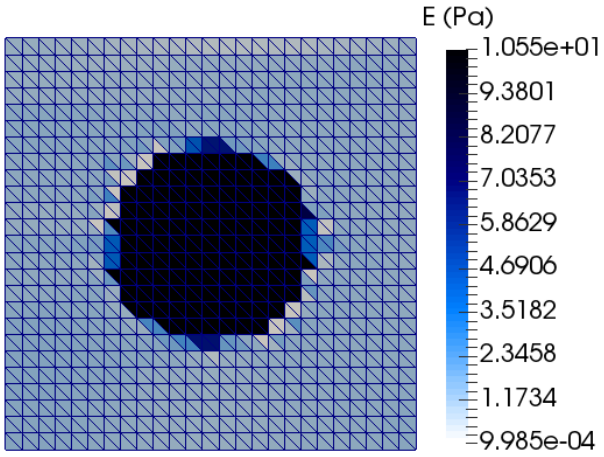

Fig. 15 Example 3 Young modulus results.

The results shown let us conclude that the proposed methodology allows to identify important information of the constitutive model even when the solid is submitted to large deformations. However, a formal extension of the method for identification of mechanical properties in nonlinear models must be developed in future works.

3.4 Example 4

In this example we solve another problem seen in the literature, where the mechanical properties and loads considered are in the order of those considered in the modeling of a carotid artery cross section with a considerable stenosis. The example is inspired in the analysis presented in [30], however the hypothesis that we will consider are similar to those assumed in [18].

The geometry of the problem can be seen in Figure 16, where the domain is divided in 16 partitions. Two supports are considered so that rigid movements are eliminated and a uniform internal pressure $q = 5$ kPa is applied as can be seen in the figure. The finite

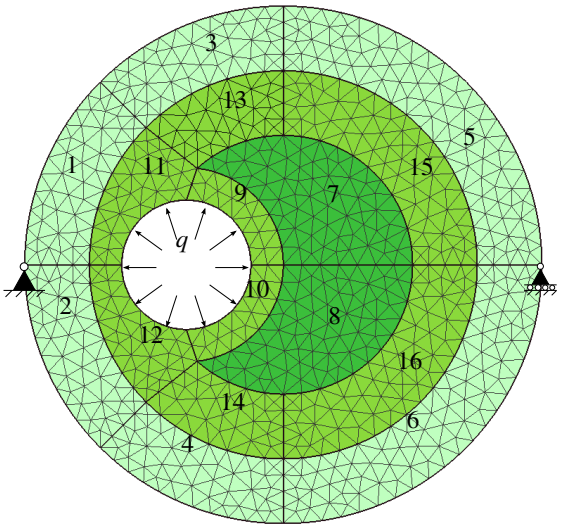

Fig. 16 Example 4 geometry, boundary conditions and mesh formed by 1492 elements with 16 partitions.

element mesh used to solve the inverse problem is formed by 1492 triangular elements.

The considered mechanical properties correspond to three materials associated with arterial wall components. The exterior ring is considered as healthy tissue, or healthy artery (HA) and its Young modulus value is $E_{\text{HA}} = 600$ kPa, in the figure this region corresponds to the partitions 1 to 6. Then, in contact with this region we consider diseased tissue (DT) with a slightly superior Young modulus $E_{\text{DT}} = 800$ kPa, in the region formed by the partitions 9 to 16. Finally we find a lipidic core (LC) where a low Young modulus is considered $E_{\text{LC}} = 10$ kPa, in the partitions 7 and 8. As it is considered in [18] a plane strain state is assumed. Since the FEM analysis code solves compressible solid problems, the Poisson ratio used is $\nu = 0.3$ instead of 0.49.

The direct problem is solved using E^r and a mesh with 12770 elements and the displacements are interpolated to the mesh with 1492 elements obtaining the reference displacements $\mathbf{U}^r$. The displacements obtained when the direct problem is solved using the mesh with 1492 elements and the E^r Young modulus, present a level of error $\eta_U = 4.52\%$.

In [18] a variable E is considered for each material region of the wall, this means that three variables are considered for the identification of the whole domain. In this article we consider the same three groups considered in the paper cited and also consider 16 element groups defined by the partitions in Figure 16. Finally we will consider one Young modu-

lus variable for each element of the mesh. In the first two cases no regularization will be applied, since the grouping of elements might produce a regularization effect. In a real life application this grouping of elements might be justified by a previous appropriate image segmentation, where different structures could be recognized. In the following we present the results obtained when the identification is performed using each one of these three element grouping. The identifications are performed using Sedumi with the same parameters as in the previous examples.

Identification with three groups Let us consider now that the elements are grouped as follows: HA includes the elements in the partitions 1 to 6, LC includes the elements in the partitions 7 and 8, and DT includes the partitions 9 to 16. The identification is performed using the formulation CPCEG without regularization term, the minimum and maximum Young modulus values are $E_{\min} = 10$ Pa and $E_{\max} = 10^9$ Pa. One variable E is considered for each group, it means that three values E will be identified.

In Table 5 the identification results are presented, where the Young modulus obtained are E^* and the relative error is calculated as $\delta E = \frac{|E^* - E^r|}{E^r}$. We can see that the error obtained

Region	E^r (kPa)	E^* (kPa)	$\delta E(\%)$
HA	600	581.66	3.06
LC	10	8.90	11.00
DT	800	764.82	4.40

Table 5 Example 4 results with 3 element groups.

in the values E is acceptable, thus we confirm that the grouping of elements produce a regularization effect.

Identification with 16 *element groups* Let us now consider that each one of the partitions shown in Figure 16 will have one Young modulus variable to identify. Once again the identification is performed with the same parameters as above.

In Table 6 we see the results obtained for each group of elements. In this case we obtain slightly higher errors than in the previous case. In Figure 17(a) the plots of the Young modulus obtained after the identification are presented. In Figure 17(b) the plots of the absolute value of the relative error are presented. We see that the partitions with higher error are the 13 and 14, and in second place we see the 7 and 8. Although errors are present in the solutions, we remark that the stiffness relations between different partitions is conserved, providing a reasonable identification.

Identification without groups Finally in this case the identification is performed considering one Young modulus variable per each element, which means that no grouping is applied. In this case regularization must be applied.

Region	E^r (kPa)	E^* (kPa)	$\delta E(\%)$
1	600	568.41	5.27
2	600	568.39	5.27
3	600	560.06	6.66
4	600	559.96	6.67
5	600	568.65	5.22
6	600	568.63	5.23
7	10	8.42	15.76
8	10	8.42	15.76
9	800	773.22	3.35
10	800	773.34	3.33
11	800	764.63	4.42
12	800	764.63	4.42
13	800	629.80	21.28
14	800	629.89	21.26
15	800	728.04	8.99
16	800	728.00	9.00

Table 6 Example 4 results using 16 elements groups.

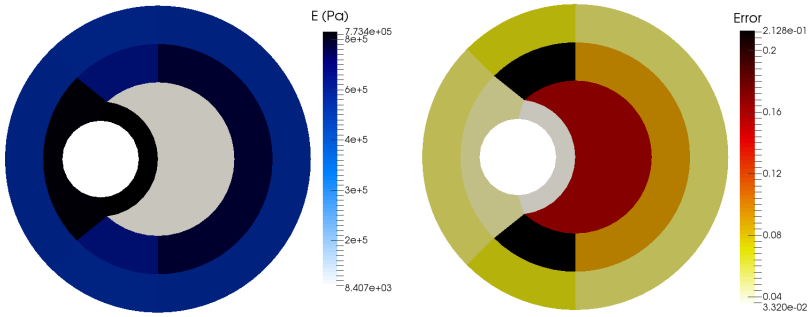

(a) Young modulus (b) Relative errors

Fig. 17 Example 4 results for 16 element groups.

In this case the methodology presented does not provide a solution for which the interfaces to the right of the domain can be correctly identified. In order to see if the low quality of the solution is related to the Morozov criterion, solutions were obtained for α in a wide range of values. The results obtained show that in this example there is no value α for which all the material interfaces can be identified. In Figure 18(b) a solution obtained using a relatively large value α is shown. In this case only the interfaces located to the left of the domain can be detected. As the value α decreases the solutions become similar to the material distribution shown in Figure 18(a). The error plots are presented in Figure 19. It is observed that the solution looses regularity (the field E presents large oscillations) to the left of the domain. This loss of regularity occurs before the interfaces to the right can be

identified. Therefore, with the error introduced in the measurements and the regularization considered, there is no value α such that all the interfaces of the reference solution can be adequately identified.

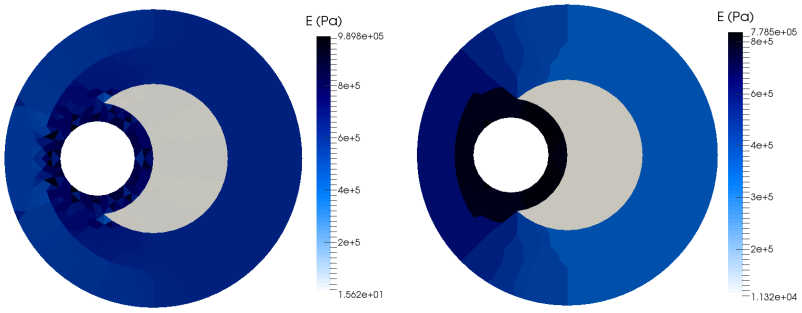

(a) Youngs obtained with $\alpha = 10^{-7}$ (b) Youngs obtained with $\alpha = 3.0 \times 10^{-6}$

Fig. 18 Example 4 Young modulus results without groups of elements.

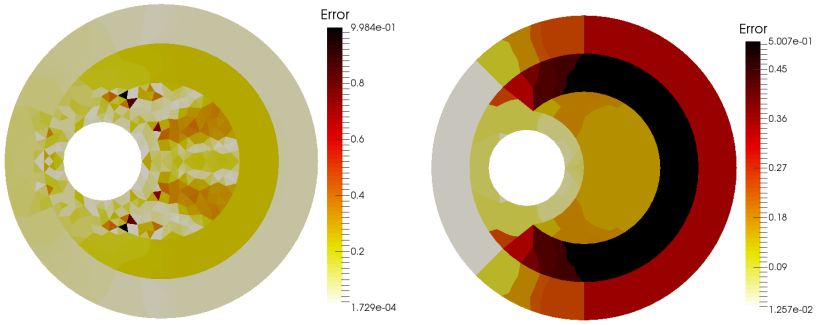

(a) Errors for $\alpha = 10^{-7}$ (b) Errors for $\alpha = 3.0 \times 10^{-6}$

Fig. 19 Example 4 relative errors results without groups.

Looking at the results we can say that this example represents a challenge for identification methods with the regularization technique applied. The authors have not seen this example solved using one variable E per element in the literature.

Execution times In Table 7 we see the times required for each identification grouping scheme. Since the software and computers used for this article are not the same as those used in [18] it is not possible to do a direct comparison of the times of execution. However, we can consider as a reference the time required to solve the direct problem (FEM analysis), and look at the relation with the identification time. In the table t_I/t_A represents the time required for

Scheme	time (s)	t_I/t_A
analysis	0.56	-
3 groups	26.1	46.6
16 groups	29.7	53.0
no groups	276.1	493.0

Table 7 Example 3 identification times.

identification over the time required for analysis. The direct problem solved in [18] involves higher complexity due to the constitutive model, the finer mesh and the order of the elements used. However, the time required for each FEM analysis is similar to the time required by the code used in this paper, showing that the tools used in this work provide a lower performance. Taking this into account we can reinforce the conclusion about the efficiency of the formulation CPCEG.

4 Conclusions

Two new formulations of the material identification problem using full-field displacement measurements were presented. The first one, called CPCEG, defines a second order cone optimization problem, while the second one, called QPCEG, defines a convex quadratic programming problem. Thefore, both formulations are based on convex optimization problems which can be solved using efficient interior-point algorithms. It was shown that the use of these approaches leads to a considerable reduction in the time of resolution when compared against other currently used formulations. In addition, it was shown how the TV regularization technique can be applied without losing the key features of the proposed formulations. The Morozov criterion was applied to define a suitable value for the regularization parameter.

The proposed formulation CPCEG is based in the CEGM and, since they are both equivalent, theoretical results support the application of the CPCEG. The QPCEG was obtained as a modified formulation of the CEGM and although there are no theoretical results supporting its use, the numerical results obtained in Example 1 show that this formulation produces solutions of similar quality to those provided by the CPCEG, requiring even lower execution times.

It was shown that the formulations CPCEG and QPCEG can obtain solutions for the MIP appropriate for material identification even when the measurements have random and interpolation error. Although both formulations are able to solve large problems, the QPCEG requires less computational resources, therefore if low memory resources are available the QPCEG might be a good alternative. It is important to remark that a solution with a slightly higher error was obtained when using QPCEG. In short, the formulation QPCEG showed

promising results in terms of precision and computational costs. However, theoretical aspects of this formulation must be addressed in future studies.

In Example 3 it was shown that the proposed method allows to identify important features of the solution even when the solid is submitted to large deformations. An extension of the method for identification of mechanical properties of nonlinear models must be developed in future works.

The results obtained for Example 4 show that the geometry and the values of material properties of the stenosed arterial cross section are very difficult to identify correctly, even when a low error is considered. The grouping of elements leads to a better identification, but such technique is possible only if a priori information is available, e.g. a reliable image segmentation.

Since Example 4 is inspired in a cardiovascular disease diagnosis problem, the search for more effective formulations must be continued in future works. For instance, the proposed formulations could be generalized to consider several load cases. Extensions for the identification of material properties of anisotropic elastic or viscoelastic materials must be also studied in future works.

Acknowledgements This research was financially supported by the Uruguayan National Research and Innovation Agency (ANII: project codes FMV-3-2011-1-6125 and POS-2011-1-3570) and the "Comisión Sectorial de Investigación Científica (CSIC)".

References

1. Auger, A., Hansen, N., Perez Zerpa, J.M., Ros, R., Schoenauer, M.: Experimental Comparisons of Derivative Free Optimization Algorithms. In: Lecture Notes in Computer Science, vol. 5526 LNCS, pp. 3–15. Springer (2009). DOI 10.1007/978-3-642-02011-7{_}3. URL http://link.springer.com/10.1007/978-3-642-02011-7{_}3
2. Avril, S., Badel, P., Duprey, A.: Anisotropic and hyperelastic identification of in vitro human arteries from full-field optical measurements. Journal of Biomechanics **43**(15), 2978–2985 (2010). DOI 10.1016/j.jbiomech.2010.07.004. URL http://www.ncbi.nlm.nih.gov/pubmed/20673669http://linkinghub.elsevier.com/retrieve/pii/S0021929010003738
3. Avril, S., Bonnet, M., Bretelle, A.S., Grédiac, M., Hild, F., Ienny, P., Latourte, F., Lemosse, D., Pagano, S., Pagnacco, E., Pierron, F.: Overview of Identification Methods of Mechanical Parameters Based on Full-field Measurements. Experimental Mechanics **48**(4), 381–402 (2008). DOI 10.1007/s11340-008-9148-y. URL http://link.springer.com/10.1007/s11340-008-9148-y
4. Ayachit, U.: The ParaView Guide: A Parallel Visualization Application. Kitware, Incorporated (2015)
5. Banerjee, B., Walsh, T.F., Aquino, W., Bonnet, M.: Large scale parameter estimation problems in frequency-domain elastodynamics using an error in constitutive equation functional. Computer Methods in Applied Mechanics and Engineering **253**, 60–72 (2013). DOI 10.1016/j.cma.2012.08.023. URL http://www.pubmedcentral.nih.gov/articlerender.fcgi?artid=3501763{&}tool=pmcentrez{&}rendertype=abstracthttp://linkinghub.elsevier.com/retrieve/pii/S0045782512002770

6. Barbone, P.E., Gokhale, N.H.: Elastic modulus imaging: on the uniqueness and nonuniqueness of the elastography inverse problem in two dimensions. Inverse Problems **20**(1), 283–296 (2004). DOI 10.1088/0266-5611/20/1/017. URL http://stacks.iop.org/0266-5611/20/i=1/a=017?key=crossref.d13f22fe48062b2a982ee068f0b414ff
7. Beck, A., Ben-Tal, A., Tetruashvili, L.: A sequential parametric convex approximation method with applications to nonconvex truss topology design problems. Journal of Global Optimization **47**(1), 29–51 (2009). DOI 10.1007/s10898-009-9456-5. URL http://link.springer.com/10.1007/s10898-009-9456-5
8. Ben-Tal, A., Nemirovski, A.: Lectures on modern convex optimization: analysis, algorithms, and engineering applications. Society for Industrial and Applied Mathematics (2001). URL http://citeseerx.ist.psu.edu/viewdoc/summary?doi=10.1.1.134.932$\backslash$nhttp://books.google.com/books?hl=en{&}lr={&}id=M3MqpEJ3jzQC{&}oi=fnd{&}pg=PR11{&}dq=Lectures+on+modern+convex+optimization+analysis+algorithms+and+engineering+applications{&}ots=O3kXEzlTWO{&}sig=pCxNy7L7k
9. Bonnet, M., Constantinescu, A.: Inverse problems in elasticity. Inverse Problems **21**(2), R1–R50 (2005). DOI 10.1088/0266-5611/21/2/R01. URL http://stacks.iop.org/0266-5611/21/i=2/a=R01?key=crossref.bba85b522a27b076dd96d50bff83e189
10. Canelas, A., Laurain, A., Novotny, A.A.: A new reconstruction method for the inverse potential problem. Journal of Computational Physics **268**, 417–431 (2014). DOI 10.1016/j.jcp.2013.10.020. URL http://www.sciencedirect.com/science/article/pii/S0021999113006967http://linkinghub.elsevier.com/retrieve/pii/S0021999113006967
11. Chandran, K., Mun, J., Choi, K., Chen, J., Hamilton, A., Nagaraj, A., McPherson, D.: A method for in-vivo analysis for regional arterial wall material property alterations with atherosclerosis: preliminary results. Medical Engineering & Physics **25**(4), 289–298 (2003). DOI 10.1016/S1350-4533(02)00224-2. URL http://linkinghub.elsevier.com/retrieve/pii/S1350453302002242
12. Cottin, N., Felgenhauer, H.P., Natke, H.G.: On the parameter identification of elastomechanical systems using input and output residuals. Ingenieur-Archiv **54**(5), 378–387 (1984). DOI 10.1007/BF00532820. URL http://link.springer.com/article/10.1007/BF00532820http://link.springer.com/10.1007/BF00532820
13. Curnier, A.: Computational Methods in Solid Mechanics. Springer (1994)
14. De Korte, C.L., Pasterkamp, G., van der Steen, A.F.W., Woutman, H.A., Bom, N.: Characterization of Plaque Components With Intravascular Ultrasound Elastography in Human Femoral and Coronary Arteries In Vitro. Circulation **102**(6), 617–623 (2000). DOI 10.1161/01.CIR.102.6.617. URL http://www.ncbi.nlm.nih.gov/pubmed/10931800http://circ.ahajournals.org/cgi/doi/10.1161/01.CIR.102.6.617
15. Doyley, M.M.: Model-based elastography: a survey of approaches to the inverse elasticity problem. Physics in Medicine and Biology **57**(3), R35–R73 (2012). DOI 10.1088/0031-9155/57/3/R35. URL http://www.pubmedcentral.nih.gov/articlerender.fcgi?artid=3374584{&}tool=pmcentrez{&}rendertype=abstracthttp://stacks.iop.org/0031-9155/57/i=3/a=R35?key=crossref.7ae4f9dca2362a456e81960acc8e7269
16. Doyley, M.M., Meaney, P.M., Bamber, J.C.: Evaluation of an iterative reconstruction method for quantitative elastography. Physics in Medicine and Biology **45**(6), 1521–1540 (2000). DOI 10.1088/0031-9155/45/6/309. URL http://stacks.iop.org/0031-9155/45/i=6/a=309?key=crossref.9194c8e8a482d0463d79d0c647143fd0
17. Florentin, E., Lubineau, G.: Identification of the parameters of an elastic material model using the constitutive equation gap method. Computational Mechanics **46**(4), 521–531 (2010). DOI 10.1007/s00466-010-0496-y. URL http://link.springer.com/10.1007/s00466-010-0496-y
18. Franquet, A., Avril, S., Le Riche, R., Badel, P.: Identification of heterogeneous elastic properties in stenosed arteries: a numerical plane strain study. Computer methods in biomechanics and biomedical

engineering **15**(1), 49–58 (2012). DOI 10.1080/10255842.2010.547192. URL http://www.ncbi.nlm.nih.gov/pubmed/21607891

19. Franquet, A., Avril, S., Le Riche, R., Badel, P., Schneider, F.C., Li, Z.Y., Boissier, C., Favre, J.P.: A new method for the in vivo identification of mechanical properties in arteries from cine MRI images: Theoretical framework and validation. IEEE Transactions on Medical Imaging **32**(8), 1448–1461 (2013). DOI 10.1109/TMI.2013.2257828. URL http://www.ncbi.nlm.nih.gov/pubmed/23591477
20. Geuzaine, C., Remacle, J.F.: Gmsh: a three-dimensional finite element mesh generator with built-in pre- and post-processing facilities. International Journal for Numerical Methods in Engineering **79**(11), 1309–1331 (2009). DOI 10.1002/nme.2579
21. Geymonat, G., Pagano, S.: Identification of Mechanical Properties by Displacement Field Measurement: A Variational Approach. Meccanica **38**(5), 535–545 (2003). DOI 10.1023/A:1024766911435. URL http://link.springer.com/article/10.1023/A:1024766911435http://link.springer.com/10.1023/A:1024766911435
22. Goenezen, S., Barbone, P., Oberai, A.A.: Solution of the nonlinear elasticity imaging inverse problem: The incompressible case. Computer methods in applied mechanics and engineering **200**(13-16), 1406–1420 (2011). DOI 10.1016/j.cma.2010.12.018. URL http://www.pubmedcentral.nih.gov/articlerender.fcgi?artid=3096531{&}tool=pmcentrez{&}rendertype=abstract
23. Goenezen, S., Dord, J.F., Sink, Z., Barbone, P.E., Jiang, J., Hall, T.J., Oberai, A.A.: Linear and Nonlinear Elastic Modulus Imaging: An Application to Breast Cancer Diagnosis. IEEE Transactions on Medical Imaging **31**(8), 1628–1637 (2012). DOI 10.1109/TMI.2012.2201497. URL http://www.pubmedcentral.nih.gov/articlerender.fcgi?artid=3698046{&}tool=pmcentrez{&}rendertype=abstracthttp://ieeexplore.ieee.org/lpdocs/epic03/wrapper.htm?arnumber=6205627
24. Kaipio, J.P., Somersalo, E.: Statistical and Computational Inverse Problems, *Applied Mathematical Sciences*, vol. 160. Springer-Verlag, New York (2005). DOI 10.1007/b138659. URL http://link.springer.com/10.1007/b138659
25. Kallel, F., Bertrand, M.: Tissue elasticity reconstruction using linear perturbation method. IEEE Transactions on Medical Imaging **15**(3), 299–313 (1996). DOI 10.1109/42.500139. URL http://ieeexplore.ieee.org/lpdocs/epic03/wrapper.htm?arnumber=500139
26. Kavanagh, K.T., Clough, R.W.: Finite element applications in the characterization of elastic solids. International Journal of Solids and Structures **7**(1), 11–23 (1971). DOI 10.1016/0020-7683(71)90015-1. URL http://linkinghub.elsevier.com/retrieve/pii/0020768371900151
27. Kirsch, A.: An introduction to the mathematical theory of inverse problems. Springer (2011). URL http://books.google.com/books?hl=en{&}lr={&}id=RTo9ZFaSSugC{&}oi=fnd{&}pg=PR5{&}dq=An+introduction+to+the+Mathematical+Theory+of+Inverse+Problems{&}ots=hOST0HOMm{_}{&}sig=kh-NOMtJqLN4mL2g2AGdwke2Pls
28. Ladeveze, P., Leguillon, D.: Error Estimate Procedure in the Finite Element Method and Applications (1983). DOI 10.1137/0720033
29. Lee, S.Y., Rus, G., Park, T.: Detection of stiffness degradation in laminated composite plates by filtered noisy impact testing. Computational Mechanics **41**(1), 1–15 (2007). DOI 10.1007/s00466-007-0164-z
30. Li, Z.Y., Tang, T., U-King-Im, J., Graves, M., Sutcliffe, M., Gillard, J.H.: Assessment of carotid plaque vulnerability using structural and geometrical determinants. Circulation journal : official journal of the Japanese Circulation Society **72**(7), 1092–1099 (2008). DOI 10.1253/circj.72.1092. URL http://www.ncbi.nlm.nih.gov/pubmed/18577817
31. Lubineau, G., Florentin, E.: The global equilibrium method and its hybrid implementation for identifying heterogeneous elastic material parameters. Computers & Structures **89**(7-8), 656–667 (2011). DOI 10.1016/j.compstruc.2011.01.010. URL http://linkinghub.elsevier.com/retrieve/pii/S0045794911000113
32. Luenberger, D.G., Ye, Y.: Linear and Nonlinear Programming, 3 edn. Springer (2008)

33. McLaughlin, J.R., Yoon, J.R.: Unique identifiability of elastic parameters from time-dependent interior displacement measurement. Inverse Problems **20**(1), 25–45 (2004). DOI 10.1088/0266-5611/20/1/002. URL http://iopscience.iop.org/0266-5611/20/1/002/http://stacks.iop.org/0266-5611/20/i=1/a=002?key=crossref.7f848087db2830ff416f70650c489580
34. Moussawi, A., Lubineau, G., Florentin, E., Blaysat, B.: The constitutive compatibility method for identification of material parameters based on full-field measurements. Computer Methods in Applied Mechanics and Engineering **265**, 1–14 (2013). DOI 10.1016/j.cma.2013.06.003. URL http://dx.doi.org/10.1016/j.cma.2013.06.003
35. Ophir, J., Céspedes, I., Ponnekanti, H., Yazdi, Y., Li, X.: Elastography: a quantitative method for imaging the elasticity of biological tissues. Ultrasonic imaging **13**(2), 111–34 (1991). URL http://www.ncbi.nlm.nih.gov/pubmed/1858217
36. Pagano, S., Bonnet, M.: Constitutive Equation Gap. In: M. Grédiac, F. Hild, A. Pineau (eds.) Full-Field Measurements and Identification in Solid Mechanics, chap. 10, pp. 275–300. John Wiley & Sons, Inc., Hoboken, NJ USA (2012). DOI 10.1002/9781118578469.ch10. URL http://onlinelibrary.wiley.com/doi/10.1002/9781118578469.ch10/summaryhttp://doi.wiley.com/10.1002/9781118578469
37. Pagnacco, E., Moreau, A., Lemosse, D.: Inverse strategies for the identification of elastic and viscoelastic material parameters using full-field measurements. Materials Science and Engineering: A **452-453**, 737–745 (2007). DOI 10.1016/j.msea.2006.10.122. URL http://linkinghub.elsevier.com/retrieve/pii/S0921509306023070
38. Stull, C.J., Earls, C.J., Koutsourelakis, P.S.: Model-based structural health monitoring of naval ship hulls. Computer Methods in Applied Mechanics and Engineering **200**(9-12), 1137–1149 (2011). DOI 10.1016/j.cma.2010.11.018
39. Sturm, J.F.: Using SeDuMi 1.02, A Matlab toolbox for optimization over symmetric cones (1999). DOI 10.1080/10556789908805766
40. Vogel, C.R.: Computational methods for inverse problems. Society for Industrial and Applied Mathematics (2002). URL http://books.google.com/books?hl=en{&}lr={&}id=SHgq5PqxEcsC{&}oi=fnd{&}pg=PR13{&}dq=Computational+Methods+for+Inverse+Problems{&}ots=WFZ75Hm{_}4e{&}sig=EPESnx-tMwuIVcHZujuuTXBgliw
41. Wang, M., Brigham, J.C.: Assessment of multi-objective optimization for nondestructive evaluation of damage in structural components. Journal of Intelligent Material Systems and Structures **25**(9), 1082–1096 (2014). DOI 10.1177/1045389X13494933. URL http://jim.sagepub.com/cgi/doi/10.1177/1045389X13494933
42. Wang, M., Dutta, D., Kim, K., Brigham, J.C.: A computationally efficient approach for inverse material characterization combining Gappy POD with direct inversion. Computer Methods in Applied Mechanics and Engineering **286**, 373–393 (2015). DOI 10.1016/j.cma.2015.01.001. URL http://dx.doi.org/10.1016/j.cma.2015.01.001http://linkinghub.elsevier.com/retrieve/pii/S004578251500002X
43. Warner, J.E., Diaz, M.I., Aquino, W., Bonnet, M.: Inverse material identification in coupled acoustic-structure interaction using a modified error in constitutive equation functional. Computational Mechanics **54**(3), 645–659 (2014). DOI 10.1007/s00466-014-1018-0